Plastic Deformation Investigation Of High Energy Input Friction

Tao Yan
Marquette University

PLASTIC DEFORMATION INVESTIGATION OF HIGH ENERGY INPUT FRICTION

By
Tao Yan, B.S., M.S.

A Dissertation Submitted to the Faculty of the
Graduate School, Marquette University,
in Partial Fulfillment of the Requirements for the
Degree of Doctor of Philosophy

Milwaukee, Wisconsin
May 2014

ABSTRACT

PLASTIC DEFORMATION INVESTIGATION OF HIGH ENERGY INPUT FRICTION

Tao Yan, B.S., M.S.

Under the supervision of Professor James A. Rice

Marquette University, 2014

In this dissertation, plastic deformation of friction surfaces under high energy input is investigated. The plastic deformation of the friction surface and subsurface was studied and models were established to estimate deformation.

In order to calculate the plastic deformation at friction surface, an algorithm based on Ramberg-Osgood relationship was generated, and a single material model was developed based on this algorithm. Work hardening caused by plastic deformation and thermal softening caused by elevated temperature were considered in the model. To validate the model, an apparatus was designed to perform friction tests under different conditions. A special steel specimen with a copper insert was prepared. A single material model was validated by the test results.

Friction materials are the composites of matrix materials, reinforcement particles, abrasive particles and lubricants. Effects of additives on plastic deformation are different. Single additive particle models were built based on the single material model to study the effect of additives on the plastic deformation of the matrix material. The most common additives, graphite and silicon were investigated. Specimen with a single additive particle were fabricated and tested. The single additive particle models were compared to experiment results. Simulation models for more complicated situations were discussed.

The research in this dissertation provides a mechanism to study complex friction materials, and provides a new method for friction material study. The models are convenient tools that could be used to study the friction mechanisms and improve the performance of friction material.

ACKNOWLEDGEMENTS

Tao Yan, B.S., M.S.

First of all, I would like to express my most sincere appreciation to Dr. James A. Rice, my academic and dissertation advisor. I wish to thank him for giving me the opportunity to begin my Ph.D. studies at Marquette University and for his wise and trusted guidance in my research direction and writing techniques throughout the entire process. I further would like to thank my committee members: Dr. Kyuil Kim, Dr. Raymond A. Fournelle, Dr. Joseph Domblesky, and Dr. Vikram Cariapa, who gave me advice and consistent support whenever I needed it.

Furthermore, I would like to thank Mr. Thomas Silman, Mr. Ray Hamilton, and Mr. Dave Gibas from Discovery Learning Laboratory.Thay have contributed with a lot of interesting discussions and valuable assistance in the experimental testing and specimen design of this research project.

Finally, I am grateful to my parents, my Wife, and my baby Katherine for their patience and *love*. Without their consistent encouragement throughout my studies, this work would never have come into existence.

Tao Yan

May, 2014

TABLE OF CONTENTS

LIST OF TABLES

LIST OF FIGURES

CHAPTER 1

Introduction

1.1 Introduction

Friction materials are the components used to transfer mechanical energy into heat by sliding contact. They can be wood, rubber, stone, metal or composite materials. During sliding, several processes occur concurrently at the friction surface, such as plastic deformation in subsurface layers, mechanical mixing, hot spot creation, oxidation, phase transformation, etc. [1]

When two materials come into contact and slide against each other, the subsurface layer of the softer material experience a structural change. These changes are mainly caused by plastic deformation and heat generated during friction. Plastic deformation is determined by the the strain[2]. During sliding, shear stress is applied on the friction surface. When shear stress reach the yield point of the material, plastic deformation will be found to a small depth in the vicinity of the surface. For metals, when the temperature increases, the mechanical properties such as yield stress and shear modulus will decrease. The heat generated by friction is absorbed by the material, so friction will enhance the magnitude of plastic deformation. [3–6]

Plastic deformation also produces debris. Debris formation as a result of plastic

deformation is governed by failure criterion. Debris usually has very high surface reactivity, and so can be oxidized easily due to the heat of friction. The debris and its oxides adhere to the friction surface, form a characteristic friction layer on the surface. The friction layer will determine the performance of friction materials. The mechanisms of friction layer formation are not fully understood due to the complexity of the phenomenon [7–10].

Because of surface roughness, friction surfaces come into contact only on summits of their highest asperities, therefore, the material is deformed and modified at these summits. The contact geometry changes constantly because of the relative movement of the surfaces as well as their deformation and wear. New asperities come into contact forming new spots of deformation and modification. The friction layer on the friction surfaces will also affect the contact locations. [11, 12]

The friction coefficient and wear rate are the most important parameters that are currently of interest. Plastic deformation and friction heat are responsible for wear mechanism transition and, therefore, the effect of these two parameters must be known. In order to understand the mechanism of friction, the complex phenomena present during wear must be fully understood.

1.2 Problem statement

Though friction materials have been used for many years, basic knowledge of their mechanisms on a micro scale is limited. In order to have a good understanding of the mechanism of the sliding process, several difficulties need to be overcome.

1. During friction sliding, there are many processes occurring concurrently on the friction surface. These processes generally do not operate independently, but will affect one another. For example, the oxide layer on the fiction surface reduces the adhesive force between the sliding bodies, which will affect the shear force between two contacting bodies, which will affect the plastic deformation of the subsurface layers. The plastic deformation on the other hand plays a key role in the production of wear debris which will become oxidized, and the cycle continues.

2. Due to the complexity of friction materials microstructure, the general rules for uniform materials are not always true. For instance, in copper-based friction materials there are iron, graphite and silicon dioxide particles in a copper matrix. Each of them has different mechanical and chemical properties and behavior at high temperatures.

3. Most of the mechanisms of sliding cannot be observed during experimentation. For example, deformation, changes of the mechanical properties of materials, chemical transformation on the friction surface and subsurface, formation of the friction layer,

etc. can be only observed after the experiment.

In summary, in order to begin to understand the mechanisms of friction , a physical model is sought that will help explain these phenomena. The model should be bases on a physical understanding of the phenomena and verified by experimental results.

1.3 Objective

In this project, the objective was to study the plastic deformation of the friction surface and subsurface will be studied and to establish a model to estimate the deformation. The model in intended to provide a mechanistic approach toward understanding the plastic deformation of friction material systems and how this deformation is affected by highly loaded sliding contact. The deformation models for a single material were generated first. Then the models for composite were established.

1.4 Organization of dissertation

The dissertation is divided into five chapters. In this chapter, the research is outlined. Chapter 2 introduces the background knowledge of plastic deformation in friction materials, and the current status of research. Chapter 3 presents the models for a single material and the validation of the model. The effect of material properties on plastic deformation will also be discussed. Model of composite is covered in Chapter 4, and the effect of additive particles on plastic deformation are also be

presented in this chapter. Chapter 5 presents the conclusions, contributions to this research and plans for future work.

CHAPTER 2

Background Review

2.1 Overview of processes during friction sliding

Friction is the resistance to the relative motion of contacting bodies [13]. Friction could be dry friction or wet friction. Dry friction describes the friction between two contacted solid bodies, and can be divided into kinetic friction and static friction. Wet friction is the friction that have some other substance, usually oil or grease, between the contacted bodies. And friction can also be divided to lubricated friction and non-lubricated friction based on the existence of lubricant.

When two surface come into contact, the charged particles from both surface will generate the electromagnetic forces. Friction force occurs when breaking the electromagnetic forces. Due to the complexity of the processes, friction can only be found empirically. The degree of friction is expressed by the friction coefficient μ, which is the ratio of the frictional force to the normal force that presses two surfaces together.(Fig 2.1)

Leonardo da Vinci [14] recorded his study of friction in his notebook five hundred years ago.

1. Frictional resistance is proportional to roughness.

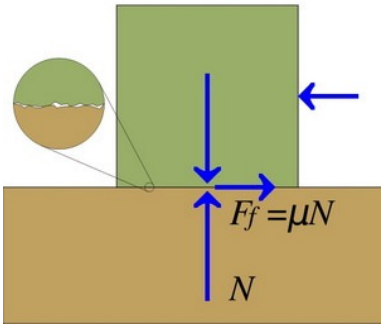

Figure 2.1: Illustration of friction force

2. Frictional resistance is doubled when the load is doubled.

3. The friction made by the same weight will be of equal resistance at the beginning of its movement although the contact may be of different breadths or lengths, which is illustrated by his drawing (Fig.2.2).

4. In friction, every body resists with 1/4 of its weight, assuming a suitable plane with a polished surface.

5. When the inclination of the polished plane enables the body to act with 1/4 of its weight in the direction of motion, the body is in itself inclined to move downward.

Amontons designed an experiment to measure friction resistance in 1699 [15]. He concluded that the resistance caused by friction is proportional to the force with which the upper surface presses against the lower; is approximately 1/3 of the force;

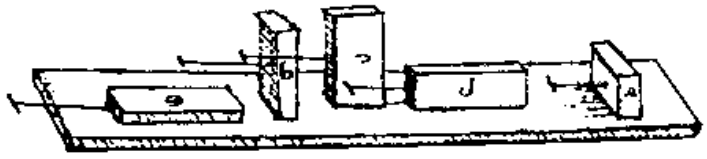

Figure 2.2: Da vincis drawing illustating his experiments on friction [14]

and is independent of the area of contact. He also found that when the surfaces were greased the resistance is independent of the nature of the surface.

In 1785, Coulomb presented a paper in which he found that in both static and kinetic friction Amontons laws concerning load and contact area were valid and the force of friction depends upon the nature of materials in contact and their coatings. He also found that the force of kinetic friction is independent of the velocity. Coulomb's ideas on the mechanism of friction are similar to those of Amontons: Friction is due to the engagement of the asperities of the surface. He suggested that part of friction force may come from the cohesion of the molecules at the sliding surface, which turns out to be a very important finding according to modern research [15].

The classic laws of sliding friction are summarized then as follows [16]:

1. Frictional force is directly proportional to normal load, that is, to the total force which acts normal to the sliding surface.

2. Frictional force for a constant load is independent of the area of contact.

3. Frictional force is independent of the velocity of sliding.

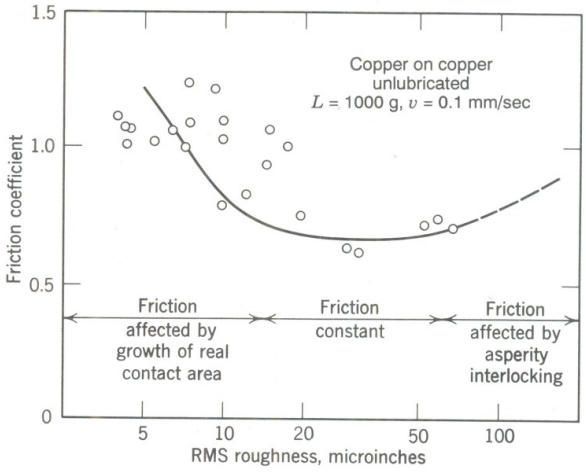

Figure 2.3: Plot of friction against roughness[18]

4. Frictional force depends upon the nature of the materials in contact.

With the development of modern experiment methods, the understanding of friction improved.

The relationship between friction coefficient and surface roughness is clear (Fig 2.3). The friction tends to be high When the surfaces are very smooth, because the real contact area is high; when the surfaces are very rough, the friction is high because the friction force needs to overcome the asperities interlocking. When roughness is in the intermediate range, the friction is at a minimum and almost independent of roughness.[17]

The understanding of the mechanism of friction resistance is improved. When one solid surface slides on another, the friction resistance comes from two processes:

the deformation of the points of actual contact and the plowing in one surface by the points of contact in the other. Tomilinsons molecular theory of friction recognizes that during sliding the frictional force is generated by overcome the bonding between two contacted surfaces, rather than the interlock effect between asperities [19]. Adhesion and plastic deformation theory was first presented in 1930s by Bowden [20, 21]. He concluded that since there is a small actual contact area, even a light load may produce a pressure high enough to cause adhesion (welding) at the point of contact. Friction resistance is due primarily to the shearing of these welds and secondarily to the work of plowing the harder material through the softer. He also postulated that increasing the applied load has the effect of increasing the actual contact area.

The dependence of friction upon velocity has been studied. During sliding, the friction coefficient decreases with sliding speed increasing when sliding speeds are low and increases when sliding speeds are high.[17] In most of the situation, the friction coefficient is considered as a constant in the velocity ranges of interest, and also is independent of the sliding velocity (Fig 2.4).[22]

With the improvement of techniques and equipment, subsequent work resulted in many important modifications to the theory. Despite the existence of experimental methods for studying physical and mechanical problems, the friction surface, especially the real contact spots between two friction components remain hard to access.

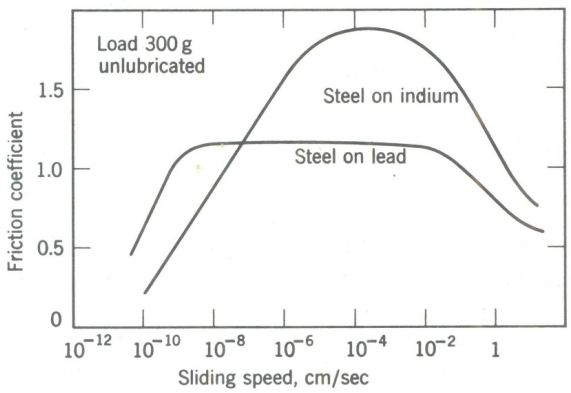

Figure 2.4: Plot of friction against sliding speed [18]

For friction material testing, the data that can be obtained during the test are coefficient of friction and the temperature measured at some distance from friction surface. All other data such as that related to the deformation, variation of material properties, chemical transformations in subsurface, transfer and mechanical mixing can be only obtained after experiment, which means researchers can only observe the consequences of phenomena and processes accurring in friction system.

During sliding, several processes occur concurrently at the friction surface, including plastic deformation in subsurface layers, mechanical mixing, hot spot creation, oxidation, etc. In order to get a good understanding of the friction process, each process must be studied separately.

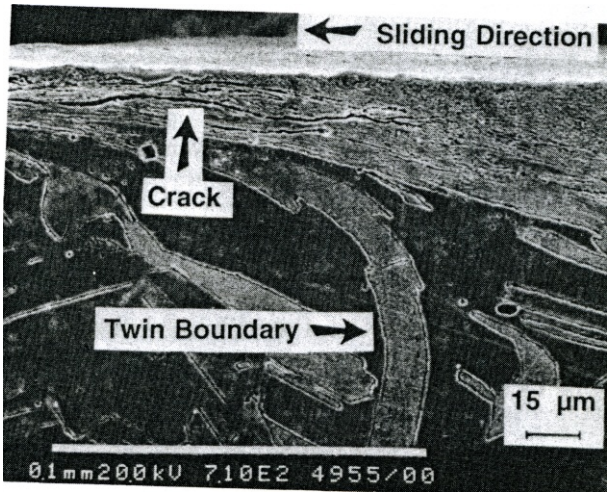

Figure 2.5: SEM image of near surface region after sliding friction [3]

2.1 Plastic deformation during sliding of metal

When a ductile material is under a mechanical load which is higher than its yield stress, shape of the material changes permanently and causes plastic deformation. Overloaded tribological components will have plastic deformation on the friction surface due to the shear stress. The heat generated at the surfaces softens the material locally, making it prone to plastic deformation.

During sliding, if the shear stress on the friction surface is exceeded the yield point of the friction material, plastic deformation will be found in the vicinity of the friction surface. Metallographic observations of the subsurface layers in Alpas's research have shown that the deformation aligned the grain structure in the sliding direction (Fig 2.5)[3].

The depth of the plastically deformed layers is determined by the sliding distance. It has been found in Alpas's research that the depth of plastically deformed layer increases with sliding distance and has a maximum value [3]. The sliding distance is not the only factor. The temperature dependence of the material's mechanical properties, such as yield stress and shear modulus, also affect the depth of deformed layer. It is difficult to observe the plastic deformation process during sliding since the deformation forms very rapidly and in most cases only the final view of the deformed structure could be obtained. The properties of these layers are always changing due to work-hardening and thermal softening.

2.1 Oxidation during sliding

In addition to the microstructural changes, chemical changes also occur on the friction surface during sliding. The oxide found on a brake pad is evidence for this. During sliding, mechanical energy is converted to heat, which is absorbed by the friction couple. The elevated temperature of the friction material makes chemical reaction possible.

Because of surface roughness, two solids contact each other on summits of their highest asperities. The material is deformed and modified at summits of the asperities in contact. Since the friction couples contact at summits of the asperities, the pressure on the contact asperities is larger than apparent pressure. This high

pressure causes plastic deformation which increases the density of dislocations on the contact asperities, resulting in the plastically deformed grains which have higher free energy. Plastic deformation also results in debris formation. Debris is usually produced in the form of small particles, which have very high surface reactivity and can be oxidized easily due to the friction heat. The change of Gibbs free energy controls the probability of ongoing reactions [10]. The total Gibbs free energy ΔG includes the contributions of mechanical energy ΔG_{mech} , the surface energy ΔG_{surf}, and the chemical contribution ΔG_{chem}

$$\Delta G = \Delta G_{mech} + \Delta G_{surf} + \Delta G_{chem} \tag{2.1.1}$$

The main chemical reaction is the oxidation of the friction materials. Take copper-based brake pad for example (Fig.2.6), the high load on the friction surface generates lots of heat and large amount of debris. The friction surface and the back side of the used pads are covered by a layer of oxide.

2.1 Mechanical mixing during sliding

It is known that the materials transfer from one surface to the other during sliding, especially in dry conditions without lubricant. An extremely finely mixed layer named "mechanically mixed layer" (MML) was observed near the wear surface [23].

During sliding, MML originates from the small asperities which form the contact spots. Under normal pressure, the asperities of two friction surfaces are interlocked.

Figure 2.6: Oxidation of brake pad

The interlocked asperities deformed in the direction of sliding due to the tangential shearing and eventually overlap. Therefore, a lamellar structure is formed. The resulting lamellar structure is a mixture of the materials from friction couples, which observed as the material is transfered across the interface [24].

The material of the MML could come from the counter face material or the environment. For example, the friction sliding in air commonly produces oxides which are then mixed mechanically with unoxidized material. The mixed material will have different mechanical properties. It could be harder than the base material, in which case can be pressed into the base material during friction. Or, it could be softer and will stay on the friction surface.

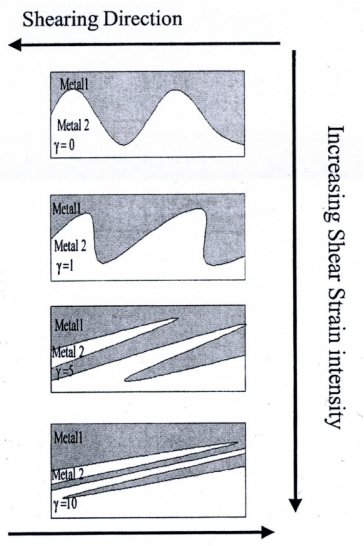

Figure 2.7: Schematic of the formation of MMLs [25]

2.1 Formation of friction layer during sliding

New brake pads usually do not have a good performance, and need a running-in process to reach a stable friction coefficient. This behavior is attributed by the formation of friction layer at the interface of friction couples. Friction layers are also called a third body or a friction film. Stable friction layers formed on a pair of friction surfaces can maintain a stable friction coefficient and wear rate [26].

The friction layer is formed during braking and is discontinuous. The wear particles compacted during friction and formed such a surface layer. The hard particles in friction materials like silica represent primary contact plateaus. The plateaus grows when wear debris are compacted around them. The thickness of the friction layer can

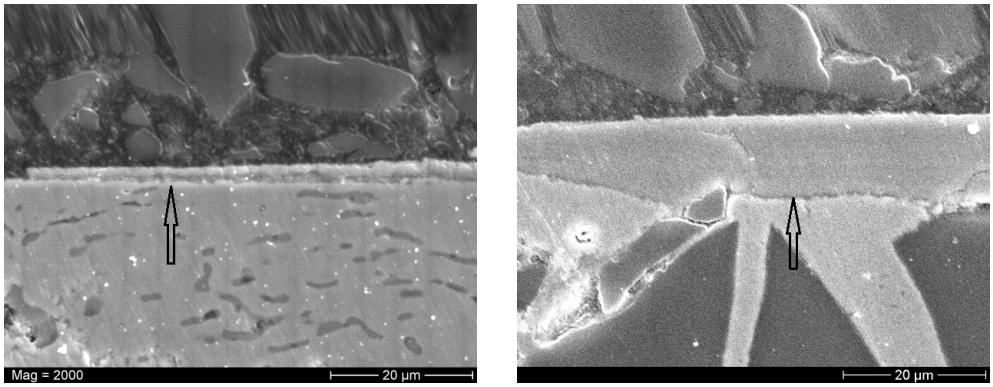

(a) Single layer (b) Double layer

Figure 2.8: Friction layers observed on copper-based friction material.

be thicker when there are grooves or pores (Fig 2.8). Running-in and fading effects can be considered as birth, growth, and degradation of such plateaus[27].

The chemical composition of the friction layer depends on the makeup of the friction materials and the environment, as well as operation conditions such as temperature. In the research of Yao Pingping [28], worn surfaces of Cu-based friction materials for aircraft were studied. Their results showed that the main components of worn surface were graphite, SiO_2, Cu, Fe and oxides of Fe (Fe_3O_4 and FeO). Graphite, SiO_2 and Cu are from the brake pad. Fe may come from both brake pad and disc. Oxides of Fe are the result of oxidation due to the high temperature.

2.1 Hot spots creation

The heat generated in friction may lead to the development of hot spots. Hot spots are high thermal gradients on the sliding surface. Hot spot creation in the

Table 2.1: Hot spots classification

Hot spots type	Width(mm)	Temperature(C)	Duration
Asperity	<1	1200(peak)	<1ms
Gradients on hot bands	5-20	650-1000	0.5-10s
Hot bands	5-50	800	>10s
Macroscopic hot spots	40-110	1100 (peak)	>10s
Regional hot spots	80-200	20-300	>10s

friction process can lead to damage and failure of the friction material.It is one of the most dangerous phenomena. It has been shown that hot spots can induce a cycling of tensile and compressive stresses with plastic strain variations [29]. Consequently, thermal cycle fatigue may occur and result in the development of cracks on the friction surface [30]. These high temperatures may also lead to poor braking performance such as brake fade and undesirable low frequency vibrations called hot judder [31].

Anderson and Knapp gave a classification of hot spots when they studied automotive friction systems (Table 2.1) [30].

2.2 Plastic deformation on the friction subsurface

Plastic deformation is observed in most materials. It describes the permanent shape changes of a material in response to applied force.

2.2 Mechanism of plastic deformation during friction

During sliding, the friction force needs to provide the energy for rupturing the adhesion junction, the plowing process, and deformation of asperities. The shear stress

produced by friction on the interface of two sliding surfaces will cause a displacement of the material under the friction surface. When the shear stress exceed the yield stress of material, plastic deformation occurs.

Experimental study of deformed surfaces in metals and alloys shows that at sliding under heavy loads plastic flow of material occurs mainly along the sliding direction. Deformation is localized in the surface layers in which laminar plastic flow of material decreases monotonously with increasing distance from the friction surface.

The plastic deformation will change the material properties and affect the performance of friction material. As such the investigation of plastic deformation during friction is important and necessary.

2.2 Real area of contact (RAC)

The surfaces of solids are not perfectly smooth at a microscopic level. When two solid materials come into contact, their surfaces will be very close at the contacting spot. These regions usually are the tips of asperities, and the pressures there are very high. Over these regions where intimate contact occurs, strong adhesion takes place. It is assumed that all of the interactions take place at these regions, called junctions, where there is atom-to-atom contact. The total areas of all junctions is the real area of contact A_r. Fig 2.9 shows a schematic drawing of the real contact area.

Assuming ideal plastic deformation, which means no work hardening during plastic

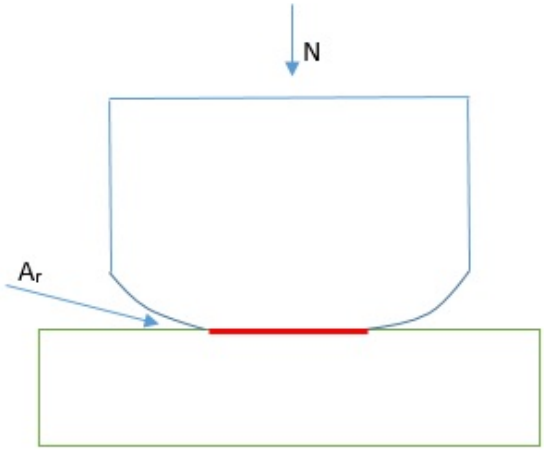

Figure 2.9: Real contact area of a microasperity

deformation, the minimum value of A_r, which turns out to be close to the actual value of real contact area, can be calculated [18].

$$A_r \geq \frac{N}{\sigma_p}, \tag{2.2.1}$$

where N is the normal force to the interface, and σ_p is the penetration hardness, which is the maximum compressive stress that material in the contact region can carry without plastic yielding. When the pressure $\frac{N}{A_r}$ is smaller than σ_p, no plastic yielding occur at the contact tip, and $A_r > \frac{N}{\sigma_p}$. When the pressure is bigger than σ_p, plastic yielding occur and the A_r increases until $A_r = \frac{N}{\sigma_p}$.

$$\sigma_p = cQ_r, \tag{2.2.2}$$

where c is a coefficient which is depends on the geometry of asperities, and Q_r is the

material's yield strength. As a first approximation, c can be taken as being equal to 3 [32]. This equation is used to calculate A_r in the following cases:

1. When the total surface of asperities is big, and consequently the surface is very smooth. The normal force applied is not big enough to cause plastic deformation.

2. When shear force as well as normal force act on a junction. When the shear force is applied, tangential motion occurs. This motion has the effect of increasing the area of contact [33].

3. When material of the junction creep. In a typical hardness test, the load is applied for about 10 seconds. Thus, for the materials that creep, A_r will be smaller than the calculated value from Eq.2.2.1 for the first 10 seconds after the load is applied, and larger than the calculated value after 10 seconds of load application.

In many cases, A_r is indeed equal to $\frac{N}{\sigma_p}$. When two solid surfaces contact each other and a normal load is applied, plastic deformation will occur. The initial contact points become contact areas, and the deformation will continue until the total real area of contact reaches a value equal to $\frac{N}{\sigma_p}$. This is experimentally proved by the electrical resistance measurement of contacting metals made by Bowden and Tabor [20].

2.2 Adhesion mechanisms of friction

The friction during sliding is caused by the effects of three processes: adhesion between the flat surfaces, abrasion by wear particles and hard surface asperities, and asperity deformation.[34]

The adhesion portion of friction is caused by rupture of the interfacial bonds formed in the real contact area. In order to make sliding taking place, the friction force needs to be strong enough to break the weakest bonds at the areas.

The adhesion component of friction can be written as [18]

$$\mu_a = \frac{F_f}{N} = \frac{\tau_s A_r}{N} = \frac{\tau_s}{\sigma_p} \tag{2.2.3}$$

Where τ_s is the shear strength at the interface, A_r is the real contact area, σ_p is the the penetration hardness.

When the surface energy of the contacting bodies is taking into account, the equation can be rewritten. In Fig.2.10, the load produces work of amount $N \cdot x$, and the material deformation uses up energy of amount $\int_0^x \pi r^2 \sigma_p d_x$. The surface energy change is $W_{12} \cdot \pi r$, where $W_{12} = \gamma_1 + \gamma_2 - \lambda_{12}$, γ_1 and γ_2 are the energies/area needed to create two surfaces, $\lambda_{12}$is the energy/area needed to destroy an interface, r is average junction radius. [18]

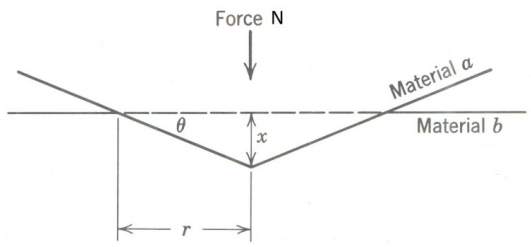

Figure 2.10: Hard cone of material a pressed into softer flat surface of material b

Then the overall energy change will be:

$$E_g = N \cdot x - \int_0^x \pi r^2 \sigma_p d_x + W_{12} \cdot \pi r^2 \tag{2.2.4}$$

Using the substitution $r = x \cdot cot\theta$, θ=average slope of asperities, and differentiating, obtain

$$\frac{dE_g}{dx} = N - \pi r^2 \sigma_p + 2\pi r W_{12} cot\theta \tag{2.2.5}$$

For equilibrium, $\frac{dE_g}{dx}$ is zero. This gives:

$$N = \pi r^2 \sigma_p - 2\pi r W_{12} cot\theta \tag{2.2.6}$$

$$\mu_a = \frac{F_f}{N} = \frac{\tau_s A_r}{N} = \frac{\tau_s}{\sigma_p}\left[1 - 2\left(\frac{W_{12} cot\theta}{r\sigma_p}\right)\right]^{-1} \tag{2.2.7}$$

With consideration of the fraction of an adhesion junction and introduction of influencing parameters such as the critical crack opening factor and the work hardening factor, the calculation of adhesion of friction on the basis of the fracture mechanics model can be written as: [35]

$$\mu_a = c\frac{\sigma_{12}\delta_c}{n^2 (NH)^{1/2}} \tag{2.2.8}$$

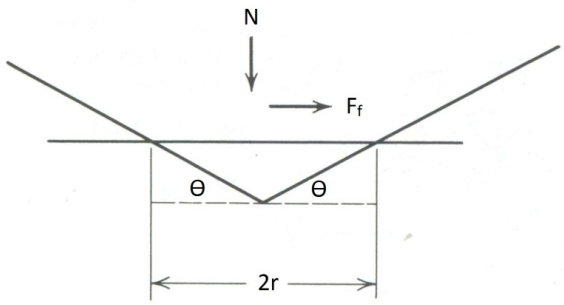

Figure 2.11: Schematic view of a cone pressed into a flat surface

where σ_{12} is interfacial tensile strength, δ_c is critical crack opening factor, n is work hardening factor, c is a constant.

2.2 Abrasion mechanisms of friction

The asperities on the surface of harder material can penetrate and plough into the softer material during sliding. Interference to the surface of the softer material can also occur as a result of impacted wear particles. During sliding, a groove is swept out of projected area A_p. (Fig. 2.11) [16]

$$A_p = \frac{1}{2} \cdot 2r \cdot r \cdot tan\theta = r^2 tan\theta \tag{2.2.9}$$

where θ is the slope of plowing asperity.

The additional resistance of sliding, due to the need to displace this area during

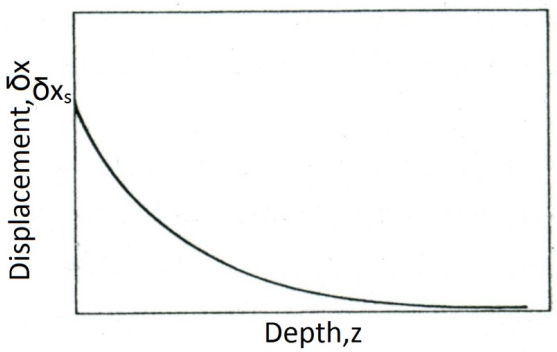

Figure 2.12: Deformation profile under friction surface

sliding, is

$$F_f = A_p \sigma_p = r^2 tan\theta \cdot \sigma_p \tag{2.2.10}$$

$$N = \pi r^2 \sigma_p \tag{2.2.11}$$

Then the plowing component of friction is:[18]

$$\mu_p = \frac{F_f}{N} = \frac{tan\theta}{\pi} \tag{2.2.12}$$

2.2 Deformation components of friction

Heilmann and Rigney [36] suggested a model for the deformation component of friction that relates friction to plastic deformation. After sliding occurs, the displacement of material is related to the depth below the material surface, which is proved by experiment (Fig.2.12).

An exponential function can be used to describe the displacement profile

$$\delta x\,(z) = \delta x_s e^{-az} \tag{2.2.13}$$

δx_s is the displacement at the surface. The shear strain increments $\Delta\gamma(z)$ decrease with depth because it is associated with the displacement. The strains can be related to displacements by:

$$\Delta\gamma(z) = -\frac{\partial}{\partial z}\delta x(z) = a\delta x_s e^{-az} \tag{2.2.14}$$

Then $\gamma(z)$ can also be described exponentially:

$$\gamma(z) = \gamma_s e^{-az} \tag{2.2.15}$$

In Heilmann's study, the relation of shear stress-strain be used is:

$$\tau = \tau_{max}\left\{1 - e^{-c\gamma}\right\}^{1/2} \tag{2.2.16}$$

The average surface strain γ_s therefore can be expressed in terms of the average surface stress τ_s :

$$\gamma_s = -\frac{1}{c} ln\left\{1 - \left(\frac{\tau_s}{\tau_{max}}\right)^{1/2}\right\} \tag{2.2.17}$$

Combining eq.2.2.15 to eq.2.2.17 give the expression of the shear stress:

$$\tau(z) = \tau_{max}\left[1 - \left\{1 - \left(\frac{\tau_s}{\tau_{max}}\right)^2\right\}^{e^{-az}}\right]^{1/2} \tag{2.2.18}$$

The expression of plastic work is:

$$W_{pl} = \int \tau(\gamma)\,\Delta\gamma dV \tag{2.2.19}$$

where $\Delta\gamma$ is the incremental strain, δx_s is the sliding distance. Assume the average

contact area of asperities is A. A_r is the sum of contact areas of all asperities. The depth z will be the only parameter that affects the stress. Eq. 2.2.19 becomes:

$$W_{pl} = A_r \int_0^\infty \tau(\gamma)\, \Delta\gamma dz \tag{2.2.20}$$

Combine Eq. 2.2.14,2.2.18 and 2.2.20 to get:

$$W_{pl} = A_r \tau_{max} a \delta x_s \int_0^\infty \left[1 - \left\{ 1 - \left(\frac{\tau_s}{\tau_{max}} \right)^2 \right\}^{e^{-az}} \right]^{1/2} e^{-az} dz \tag{2.2.21}$$

The integral can be solved by substituting:

$$q = 1 - \left\{ 1 - \left(\frac{\tau_s}{\tau_{max}} \right)^2 \right\}^{e^{-az}} \tag{2.2.22}$$

which gives:

$$W_{pl} = \frac{A_r \tau_{max} \delta x_s}{ln\left\{1 - (\tau_s/\tau_{max})^2\right\}} \int_0^{(\tau_s/\tau_{max})^2} \frac{q^{1/2}}{q-1} dq \tag{2.2.23}$$

or

$$W_{pl} = A_r \delta x_s \tau_{max} F\left(\frac{\tau_s}{\tau_{max}} \right) \tag{2.2.24}$$

where

$$F(u) = 1 - 2\frac{ln(1+u) - u}{ln(1-u^2)}$$

During frictional, the work needed to move the material a distance δx_s is

$$W_f = \mu_d N \delta x_s \tag{2.2.25}$$

where N is the normal load applied on the friction surface. In Heilmann's model, The basic assumption is that $W_{pl} = W_f$. So, combine Eq. 2.2.24 and Eq.2.2.25, to obtain:

$$\mu_d N \delta x_s = A_r \delta x_s \tau_{max} F\left(\frac{\tau_s}{\tau_{max}} \right)$$

or

$$\mu_d = \frac{A_r}{N}\tau_{max}F\left(\frac{\tau_s}{\tau_{max}}\right) \tag{2.2.26}$$

In addition to the friction components described above, the friction force can increase when the wear debris is a viscoelastic or plastic substance that sticks to the sliding interface and undergoes repeated deformation.

2.2 Present research status of plastic deformation in the friction process

Alpas [3] and coworkers tested annealed OFHC copper samples under constant load and velocity conditions. Metallographic observations of the subsurface layer of the tested samples have shown that the equiaxed grains were plastically deformed and bent to the direction of sliding. They also found that both the amount of plastic deformation and the depth of plastically deformed layers increase with the sliding distance. Their experimental results show that maximum values of these two parameters exist for given experiment condition.

In previous research, Rubtsov and Kolubaev [11, 12] found that the plastic flow of deformed surface layers occurs mainly along the sliding direction. Deformation can be localized in the surface layer and decrease with distance from the friction surface. From a microscopic point of view, the structure and properties of the deformed layers are practically invariable in the direction parallel to the friction surface and only depend on the depth.

Based on the results and ideas, they established a one-dimensional dynamic model. In the model, the material is considered to only shear along the sliding direction, and modification of the material properties are taken into account only in the direction normal to the contact surface. The model described the deformation of a microasperity. The model only considered the microscopic characteristics of the microasperity. They also assumed that the mechanical properties of the material linearly decreased with temperature increase.

This model considered both the work-hardening effect and thermal softening effect. In Rubtsov's following research, he found that changes to the thermal state cause changes of both the magnitude of plastic shear and the depth of its penetration. In repeat contacts, the maximal increment of deformation and deformed layer thickness occurs after the first contact. As the number of contacts increases, the increment of these two values after each contact decrease. After certain number of contacts, both maximal deformation and deformed layer thickness reach their maximal values.

2.3 Powder metallurgy friction materials overview

Sintered metal based friction materials are used in clutches and brakes because of their superior mechanical and tribological properties. These materials have a metal matrix in which nonmetallic fibers, particles, and solid lubricants are dispersed. A variety of nonmetallic particles are added in different metal matrices to develop metal

Table 2.2: One formulation of copper based friction material

Component	Copper	Iron	Tin	SiO_2	Graphite	MoS_2
Weight %	61.5	18.7	5	6.2	26.4	2.2

matrix composites. The particles can be roughly divides to two groups: hard particles such as SiC, SiO_2, and Al_2O_3, and soft particles like graphite and MoS_2.[37] Copper based materials are preferred because of the high thermal conductivity.

2.3 Manufacturing process for copper based friction material

Copper based friction materials have good heat conductivity and friction resistance, so they are broadly used in brake systems. Table 2.2 presents an example of a copper based friction material formulation.

In order to achieve the desired tribological properties, iron, sand, MoS_2 and graphite are added. Depending on their purpose they can be divided into lubricating additives (MoS_2 and graphite) and friction-abrasive additives (sand). The mixed powders are compacted on a copper electroplated backing plate. Tin helps to reduce the porosity and the sintering time of Cu-based materials. It can also improve the bonding between the friction material and the backing plate.

The material was blended and graphite was added before the end of the mixing cycle in order to reduce the buildup of a barrier layer on the matrix metal particles. A binder was added to prevent segregation. The mixed powders were compacted on

the copper electroplated backing plate with pressures ranging from 165-275MPa.

Bell-type furnaces are used to sinter friction materials and the supporting steel backing plate together in a protective atmosphere. Pressure is applied on the green disks during sintering at temperatures ranging from 550°C to 950°C for times of 30 to 60 min.[38] Afterward, the sintered parts are typically machined for dimensional accuracy and surface parallelism and are usually brazed, welded, riveted, or mechanically fastened to the supporting steel members. They may also be pressure bonded directly to the assembly.

2.3 Effect of components on friction performance

Copper based friction materials generally contain several additives which have different functions. Additives can be grouped by their functions as abrasive, friction modifier, filler and reinforcement, and binder materials.

Abrasive can increase friction, clean the mating surface and control the build-up of friction film. The common abrasive additives include aluminum oxide, iron oxides, quartz, silica etc.[39–41]. Take SiO_2 for example, SiO_2 can effectively improve the abrasion properties. SiO_2 particles have high strength and hardness. So they project on the friction surface and prevent the relative movement between the friction surfaces. Furthermore, the projecting SiO_2 particles can be crushed under the friction force. The SiO_2 fragments between friction couples will causes particle abrasion,

therefore increases the wear [42].

Friction modifiers are used to lubricate or raise the friction and also could react with oxygen to help control the interfacial films. The friction modifiers include copper, graphite, metal oxides, metal sulfides, mineral fillers, molybdenum disulfide, petroleum coke, etc.[39–41, 43] The most common friction modifier is graphite, which is used as a lubricant. It can reduce the friction coefficient and wear loss.

Fillers are primarily used to maintain the overall composition of the friction materials. They can be metals, alloys, ceramics, or organic materials.[39, 40, 43] Asbestos was used in early brake materials. It is stable under to $500°C$. When temperature is higher than $500°C$, it will produce silicates which are harder and more abrasive than asbestos. [44]. Iron is an important filler in copper-based friction materials. First, iron has higher strength than copper, so iron particles will project on the friction surface during sliding, which increases the surface roughness and the friction coefficient. Second, the counterpart is usually made of steel. The adhesion between iron and iron is better than that between iron and copper. Under friction load, iron particles are likely to weld with iron in the counterpart, which also increases the friction coefficient between two friction surfaces [42].

Typical binder materials are phenolic resins, metallic alloys, and modified resins.[39, 43] Phenolic resins are usually used in automotive and truck pads. Metallic alloys are used in aircraft friction brake materials. Modified resins have altered bonding

characteristics and temperature resistance.

2.3 Effect of manufacturing parameters on friction performance

For copper-based friction material, the manufacturing parameters also affect the friction performance. These parameters include particle size, green density, sintering atmosphere, sintering time, sintering temperature, sintering pressure, etc.

Particles are sintered by atomic motion that eliminates the high surface energy associated with powder. The particle size determines the surface energy per unit volume [45]. The smaller the particle size, the higher specific surface areas, and the powder will has more energy and sinter faster. Green density is the powder density after compaction. Pressing powder before sintering reduces the porosity while increasing the dislocation population in the powder. Higher green density means lower porosity and less shrinkage occurs during sintering, and the higher dislocation density that comes with higher green density contributes to an initially faster sintering rate.

The sintering atmosphere plays a very important role in the sintering process. Since oxides are already present, a reducing atmosphere can not only provide protection from oxidation, but also reduce any existing oxides. The appropriate atmosphere can also remove the lubricants and binders used in pressing. The atmosphere can control the interstitial content in the sintered material. For example, the carbon content in iron can be controlled by the specific carbon content of the atmosphere.

Time, temperature, and pressure during sintering help to improve the diffusion process thereby affecting the properties of powder metallurgy parts. In Xiongs research [46], he found that at constant sintering temperature, the porosity, wear loss, and the friction coefficient of composite all decrease as the sintering pressure increases from 0.5MPa to 1.5MPa, but increase of sintering pressure has little effect on the microstructure and tribological characteristics of copper-based friction material. He also states that under the constant sintering pressure, the density and wear resistance of material improved remarkably when the sintering temperature was increased from $900°C$ to $930°C$.

CHAPTER 3

Establishment of Plastic Deformation Model

3.1 Description of model for pure metal

The plastic deformation model is based on Rubtsovs model. [11, 12] Layer structure is used for the plastic deformation model, and both the work-hardening effect and the thermal softening effect are considered. Under the effect of the friction force, shear parallel to the surface can occur in the microasperity which is shown in Fig 3.1 by displacing the layers relative to each other. A pair of layers is an elementary carrier of the shear. Each layer is assumed to interact only with its two nearest neighbors, which means the shear of a layer is just related to its two neighbors' shears.

Assume that the shear force applied on the microasperity is not big enough to cause plastic deformation. At the initial instant, the microasperity is elastically deformed under the action of friction force. Sliding results in heat release at the friction surface and heating of the microasperity. The heating will cause a decrease of the elastic properties (softening) of the surface layer material and lead to plastic deformation. For a short contact time at the very beginning, the temperature increase is insignificant, and the degree of softening is insufficient for plastic deformation. But with the increasing of the sliding time the increased temperature will result in the

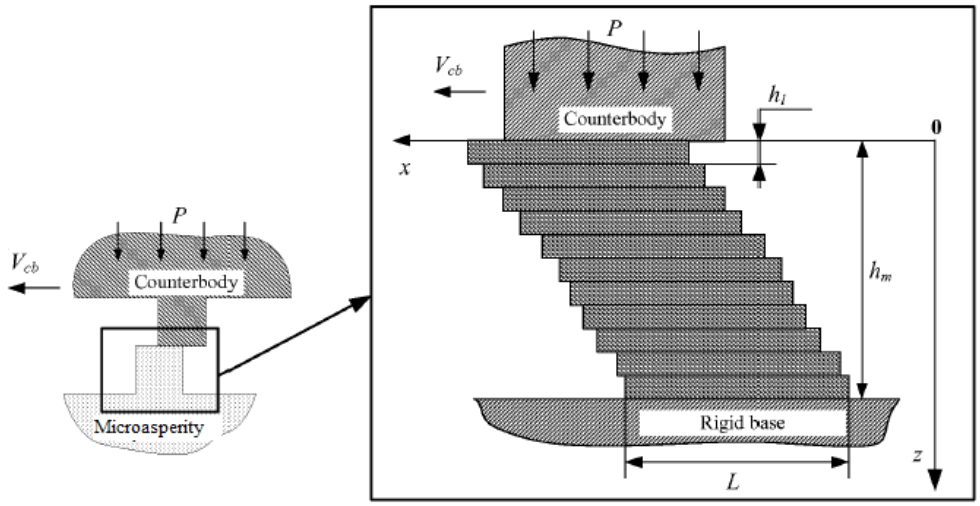

Figure 3.1: System under simulation[11]

appearance and increment of the plastic deformation.

In the simulation system, a microasperity of the height h_m is assumed as a set of layers. The layers of the material are parallel to the friction surface, and can move along the sliding direction. The layers are considered as rigid bodies and have the same length L and thickness h_l . The counterbody is assumed undeformable. The behavior of this microasperity is governed by the properties of constituent layers and the law of contact between them as well as the friction conditions. The normal contact pressure is P, and the velocity of counterbody is V_{cb}. The material of each layer is characterized by the density ρ, the specific heat c , the thermal conductivity λ, the shear modulus G, the plastic shear modulus G_{pl} responsible for strain hardening,and the yield stress in tension θ.

The equations of movement and the boundary condition for the system are written as:

$$\begin{cases} \rho^{1} h_l \dfrac{dV^1}{dt} = \tau^{fr} + \tau^{1,2} \\ \rho^{i} h_l \dfrac{dV^i}{dt} = \tau^{i,i-1} + \tau^{i,i+1} \\ \dfrac{dx^i}{dt} = V^i \\ x^k = 0 \end{cases} \tag{3.1.1}$$

Where i is the number of the layer (i=1, 2 k-1, index 1 refers to the upper layer, k is the total number of the layers); The number k layer is the base of microasperity, which is considered as rigid body and don't move during friction process. τ^{fr} is the shear stress between counterbosy and the top layer of the microasperity. The model involves the deformation criterion of plasticity. The material in a pair of neighboring layers transit from elastic to elastic-plastic deformation when the deformation at the time stage n exceeds the maximal possible elastic deformation for the given temperature in this pair.

Shear deformation in the pair of layers at the time stage n is found from the expression:

$$\gamma_n^{i,i+1} = \frac{(x_n^{i+1} - x_n^i)}{h_l} - \gamma_{n-1\ eq}^{i,i+1} \tag{3.1.2}$$

In order to find out the temperature field in the model, a one dimensional approximation is used. In this case the heat conduction equation is:

$$\rho c \dot{T} = \lambda \frac{\partial^2 T}{\partial z^2} \tag{3.1.3}$$

The boundary condition at the contact is:

$$-\lambda \frac{\partial T}{\partial z} \mid_{z=0} = W \tag{3.1.4}$$

where W is the heat flux directed from the friction surface to the microasperity. Assume that all of the friction energy is used for heating the contact pairs, and half of the heat generated on the contact surface transferred to the microasperity [6]. Then the heat flux directed to the microasperity is:

$$W = 0.5 P \mu \left| V_{cb} - V^1 \right| \tag{3.1.5}$$

V_{cb} is the velocity of counterbody, and V^1 is the velocity of the first layer on the friction surface. $|V_{cb} - V^1|$ is the relative velocity between counterbody and the microasperity. The velocity of the movement of the material on the friction surface is mostly from several hundreds of microns[47] to several centimeters [48] per second, which is small enough compared to the velocity of the counterbody.

In order to solve the temperature distribution via partial differential equations, another boundary condition needs to be set. Assume that the hight of microasperity is infinity, and the another end which has no energy input will keep a constant temperature value during the friction process. In this case the perfect heat isolation for the microasperity base gives the overestimated temperature. The overestimation can be eliminated if the assumption that the height of microasperity is infinity is made. To make the calculation feasible, the calculation region just need to exceed to the

place where the temperature dose not change during friction. Preliminary calculation shows that in this particular case, 10 times the height of the microasperity can be used as the second boundary condition.

$$\begin{cases} -\lambda \frac{\partial T_{av}}{\partial z}|_{z=0} = W_{av} = 0.5 P \mu V_{cb} \\ \\ T_{av}\left(10h_m, t\right) = T_0 \end{cases}$$

where $T_{av}\left(10h_m, t\right)$ is the average temperature at the depth $z = 10h_m$.

3.1 Improvement of the model

The model above was established based on several assumptions, including:

1. the layers are considered to be rigid bodies
2. a so-called plastic shear modulus is used as a parameter of the response function
3. all of the friction energy is transfer to heat
4. convective heat transfer was ignored
5. the mechanical properties of the material are considered to have a linear relationship with temperature

These assumptions facilitate the calculation of the model, but also introduce error in the results. The remaining portion of this chapter will focus on improvement of the model, validation of the model via experiments, and analysis of results. All of

Table 3.1: Chemical composition of SAE 1045

SAE No.	Fe	C	Mn	Si	P_{max}	S_{max}
1045	Balance	0.43/0.50	0.60/0.90	0.15/0.30	0.040	0.050

Table 3.2: Properties of SAE 1045 cold drawn steel

Property	Metric
Density	7872 kg/m^3
Modulus of elasticity	201 GPa
Specific heat capacity	486 $J/(kg \cdot K)$
Thermal conductivity	49.8 $W/(m \cdot K)$
Tensile strength	689 MPa
Yield strength	585 MPa
Elongation	16 %

the analysis is based on cold drawn AISI 1045 steel. Table 3.1 and table 3.2 give the chemical composition and properties.

3.1 Convection heat transfer

The heat source of the model is the frictional energy. Because the microasperity contacts the counterbody only on its top surface, the heat flux on the top layer is the only heat input of the model. Before sliding starts, the microasperity has the same temperature as the air. Then the first layer temperature increases due to the energy input, and the subsurface layers temperature are increased by the heat from their top neighbor layers. Temperature difference between microasperity and air will cause convection heat transfer, which is the energy output of the model.

The heat transferred from friction surface increases the temperature of the microasperity; and the heat convection on the side surface decreases the temperature of the microasperity. If only heat conduction was considered, the equilibrium status cannot be reached, even the temperature was close to the melting temperature of the material. The heat convection provide an energy output to the thermal system of the microasperity. With the consideration of heat convection, the balance point of energy input and output is exist, which make the simulation meaningful.

The convective heat flux equation is:

$$q'' = h\left(T_s - T_\infty\right) \tag{3.1.6}$$

where $q''(W/m^2)$, the convective heat flux, T_s is the surface temperature of the microasperity and T_∞ is temperature of the surrounding fluid. This expression is known as Newton's law of cooling, and the h$(W/m^2 \cdot K)$ is the convective heat transfer coefficient, which depends on conditions in the boundary layer, the nature of the fluid motion, and thermodynamic and transport properties of fluids [49]. Table 3.3 shows the typical values of the convection heat transfer coefficient.

Table 3.3: Typical values of the convection heat transfer coefficient[49]

process	h $(W/m^2 \cdot K)$
Gases (free)	2-25
Gases (forced)	25-250
liquids (free)	50-1000
liquids (forced)	100-20000
convection with phase change	2500-100000

Assuming the microasperity is a cuboid with dimension $L \cdot L \cdot h_m$, there are four side surfaces which will experience convective heat transfer. The convection will transfer heat from the microasperity into the air, change the temperature distribution of the microasperity, and consequently change the mechanical properties of the microasperity. When simulating repeated contacts, the duration of the period between contacts can be determined from the mean contact spot size and the real contact area (RCA) of the given friction pair. RCA is the sum of the areas of all the contact spots.[18] For contacts between metals the typical RCA is of the order of several percent of the apparent area. Assume the RCA is 4% and the contact spot area of microasperity can be estimated as approximately its squared size. After simple calculation it is easy to find that the duration between contact spots is 4 times as long as the contact duration. During this time, the load on the microasperity is zero, hence no heat will be generated; the only heat transfer will be the heat convection from the microasperity to the environment. The convective heat transfer is significant for microasperity; even small amount of heat loss may cause a substantial temperature decrease. So the convective heat transfer of the plastic deformation model is too important to neglect, especially when simulating repeated contacts.

3.1 Temperature dependence of mechanical properties

The mechanical properties used in this simulation model such as yield stress and shear modulus are variables of temperature. In Robtsovs work, their goal was just

to make a model, not to simulate all the properties of the material. Consequently, they assumed that the mechanical properties linearly decrease with temperature elevation, and simply took the mechanical properties at 1300 °C, which is close to the melting temperature of steel, to amount to 10% of their value at 20 °C. In the real world, however, the relationship between mechanical properties and temperature is not linear.

Take AISI 1045 steel for example. When the temperature is below recrystallization temperature (about 700°C), the yield stress decreases slowly with the increase of temperature. Once the temperature reaches recrystallization temperature, the yield stress will drop rapidly to a very low value.

To find the approximate relationship between yield stress and temperature, a simple experiment was done. The hot hardness of metal can be tested by a number of different methods. Zmeskal described the use of the Rockwell hardness tester using a Brale penetrator and mentioned that a series H Brale is suited for hot hardness tests at elevated temperatures[50]. The time is of the essence in these tests, as the specimen temperature starts to change as soon as it leaves the temperature bath. In order to increase the accuracy of results, testing should be done within 10 seconds. Rockwell B hardness of AISI 1045 steel at different temperatures was measured and converted to Vickers hardness numbers. The vickers hardness number can be related

Table 3.4: Hardness test results

T (C)	Heating	HRB	HV (kgf/mm^2)	$\sigma(MPa)$
20	HV (kgf/mm2)	97.3	224	585
50	Antifreeze Bath	97.3	224	585
75	Antifreeze Bath	96.3	218	569
100	Boiling Water	95	210	548
150	Oil Bath	91.7	193	504
200	Oil Bath	88.7	179	467
300	Muffle Furnace	86.7	171	446
350	Muffle Furnace	86.3	170	444
400	Muffle Furnace	83.3	160	418
450	Muffle Furnace	78.7	146	381

to the yield stress by

$$HV = c\sigma \tag{3.1.7}$$

where c is a constant determined by geometrical factors usually ranging between 2 and 4 [51]. So the yield stress value at different temperatures can be calculated from the hardness value at different temperature. Fig 3.2 shows the equipment used to heat the hardness specimens. Fig 3.3 shows the Rockwell hardness tester and the specimen used for hardness testing. Table 3.4 shows the hardness testing results of AISI 1045 steel at different temperatures.

The regression equation of yield stress can be expressed in two different ways. The linear regression gives the equation:

$$\sigma = -0.466T + 592, \quad R^2 = 0.9558$$

Figure 3.2: Heating Equipment

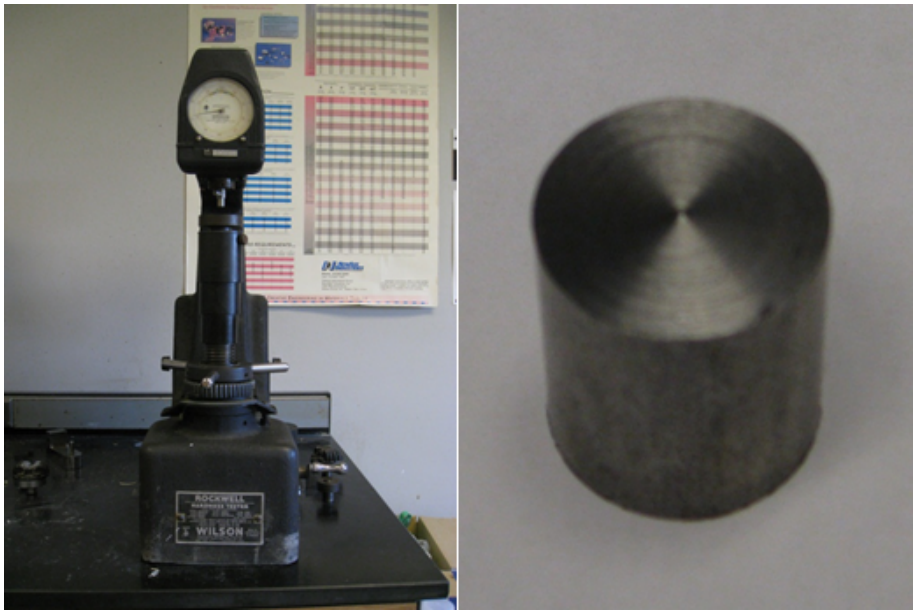

Figure 3.3: Rockwell hardness tester and specimen

Quadratic regression gives the equation:

$$\sigma = -0.00051T^2 - 0.702T + 608, \quad R^2 = 0.9684$$

By comparison, one can tell that the polynomial regression has more accurate results for the temperature dependence of yield stress. Fig 3.4 shows the two expressions.

The data points were taken in the temperature range from 20 $^\circ C$ to 450 $^\circ C$, so the quadratic regression is just valid in this range. An approximate relationship between temperature and yield stress is built, in which the first part is polynomial regression

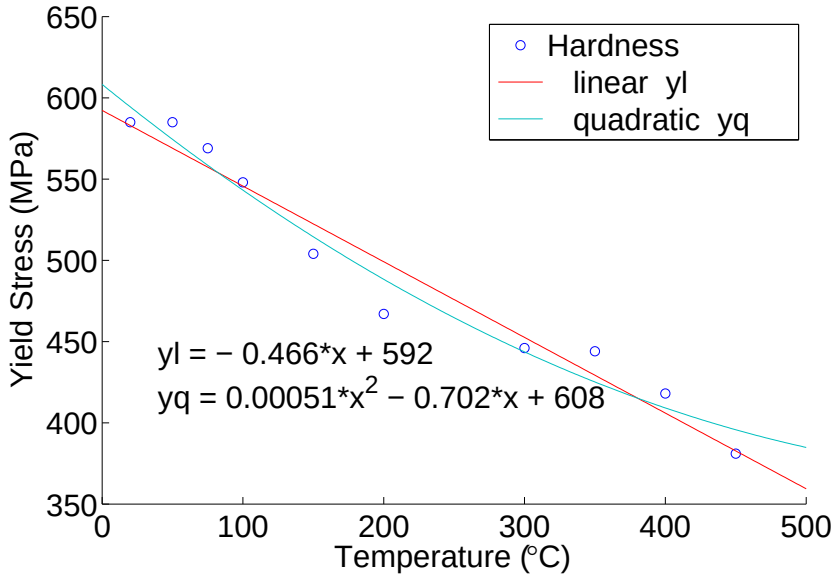

Figure 3.4: Regression of data

and the second part is linear regression. The function of the relationship is:

$$\sigma = \begin{cases} -0.00051T^2 - 0.702T + 608 & 20°C < T \leq 380°C \\ -0.466T + 592 & 380°C < T \end{cases}$$

In which T is the temperature and σ is yield stress. The plot is shown in Fig 3.5.

3.1 Calculation of temperature distribution

Based on the analysis, the temperature distribution can be calculated by:

$$\begin{cases} \rho c\dot{T} = \lambda \dfrac{\partial^2 T}{\partial z^2} \\ -\lambda \dfrac{\partial T}{\partial z} \mid_{z=0} = W = 0.5P\mu V_{cb} \\ T(H,t) = T_0 \\ q'' = h(T_s - T_\infty) \end{cases} \tag{3.1.8}$$

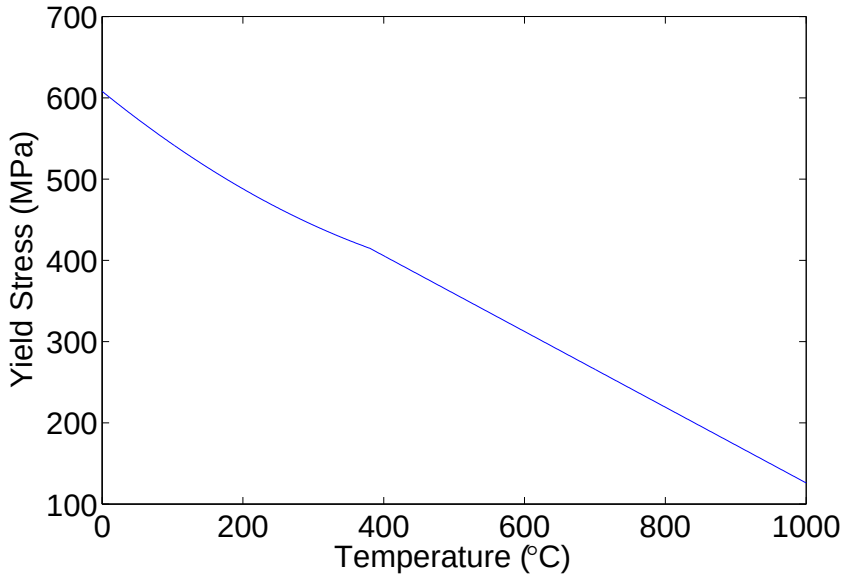

Figure 3.5: Temperature dependence of yield stress

where ρ is the density, c is the specific heat and λ is the thermal conductivity of the material. z is the depth measured from friction surface directing to the microasperity. W is the heat flux directed from the friction surface to the microasperity. It is assumed that all of the friction energy is used for heating the contact pairs, and half of the heat generated on the contact surface is transferred into the microasperity. V_{cb} is the sliding velocity of counterbody. q'' is the convective heat flux on the surface of the microasperity. h is the convection heat transfer coefficient. T_s is the surface temperature of the microasperity. T_∞ is the temperature of the air. The microasperity is assumed to be a 20mm high layered structure. Each layer has a height of $10\mu m$.

Take AISI 1045 cold drawn steel for example. The temperature distribution is

Table 3.5: Properties for temperature calculation model

Density, ρ	7872 kg/m^3
Thermal conductivity, λ	49.8 $W/(m \cdot K)$
Specific heat, c	486 $J/(kg \cdot K)$
Shear modulus, G	80 GPa
Yield stress, σ	585MPa
Pressure, P	300MPa
Sliding velocity, V_{cb}	1 m/s
Friction coefficient μ	0.5

calculated, and the result is shown in Fig 3.6; the temperature of the subsurface layers is increased with increasing contact duration, and the depth of heated layers is increased as well. This means the contact duration affects the thermal state during friction significantly. Table 3.5 shows the properties of the material at the beginning of the simulation which has a temperature of 20°C and testing condition of the simulation. The mechanical properties of the material are affected by temperature, and will change with temperature.

3.1 Calculation of plastic deformation

In order to find the shear strain in the pair of layers, the response function is used. An equation is created to present the non-linear relationship between shear stress and shear strain, which is like the Ramberg-Osgood equation[52]:

$$\gamma = \frac{\tau}{G} + K\left(\frac{\tau}{G}\right)^n \tag{3.1.9}$$

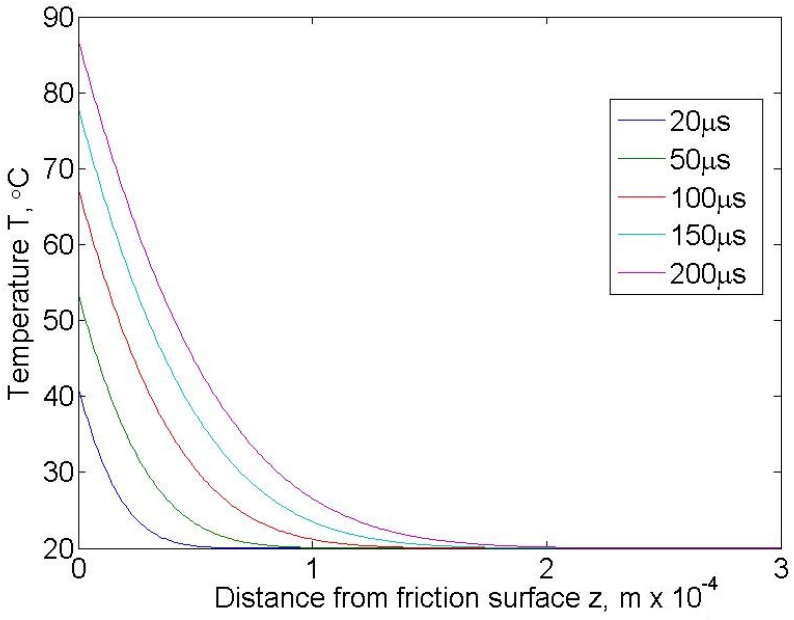

Figure 3.6: Effect of contact duration on temperature

where γ is shear strain, τ is shear stress, G is shear modulus, and K and n are constants that depend on the material being considered. The first term on the right side, τ/G, is equal to the elastic part of the shear strain, while the second term, $K\,(\tau/G)^n$, accounts for the plastic part, and the parameters K and n describe the hardening behavior of the material.

The general pattern of the response function for describing the deformation at a constant temperature is shown in Fig 3.7. The segment AB corresponds to linear-elastic behavior in a material with shear modulus G . The segment BC correspond to elastic-plastic deformation with hardening. Equilibrium shear γ_{eq} is responsible for the accumulated plastic deformation. Under equilibrium shear the stress in the pair

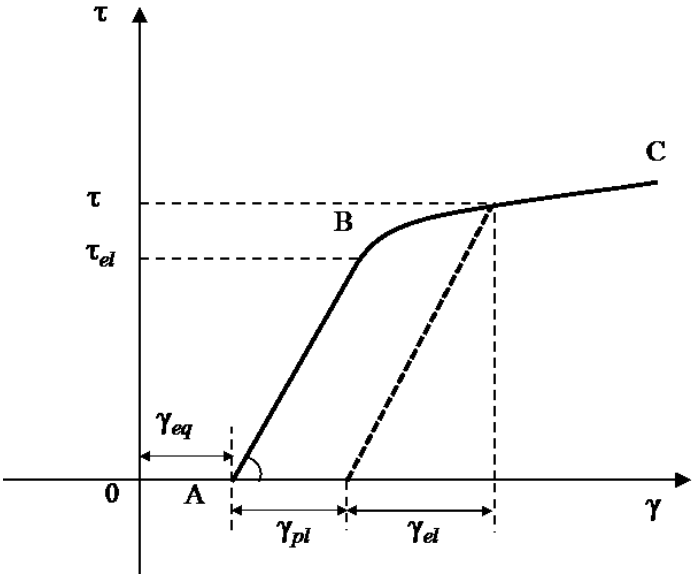

Figure 3.7: Schematic diagram of response function

of layers equals zero. For each pair of layers, the response function has its own values of the parameters which can vary during simulation. All parameters of the response function are temperature dependent, while γ_{eq} and γ_{el} also depend on their values during the previous time period.

Introducing the shear yield stress τ_y, and defining a new parameter α , which is related to K as $\alpha = K\left(\tau_y/G\right)^{n-1}$, equation (3.1.9) can be written as:

$$\gamma = \frac{\tau}{G} + \alpha\left(\frac{\tau_y}{G}\right)\left(\frac{\tau}{\tau_y}\right)^n \tag{3.1.10}$$

So the hardening behavior of the material depends on the material constants α and n. When $\tau = \tau_y$,

$$\gamma = \left(1+\alpha\right)\tau_y/G$$

From Fig 3.7, one can tell that the elastic strain at the yield point is τ_y/G and plastic strain is $\alpha\left(\tau_{y/G}\right)$. When yield stress was reached, 0.2% of offset will be left if release the load. Which means the plastic strain of the material at yield point can be expressed as:

$$\gamma_{pl} = \alpha\left(\frac{\tau_y}{G}\right) = 0.002$$

Therefore, equation (3.1.10) can be written as:

$$\gamma = \frac{\tau}{G} + 0.002\left(\frac{\tau}{\tau_y}\right)^n \tag{3.1.11}$$

Consider the strain rate effect, yield shear stress will be modified to $\tau_y^{'} = \tau_y\dot{\gamma}^m$. So:

$$\gamma_{pl} = 0.002\left(\frac{\tau}{\tau_y\dot{\gamma}^m}\right)^n \tag{3.1.12}$$

Commonly used values for n are 5 or greater [52], more precise values can be obtained by fitting the experimental data. The methods of getting a precise value for n is not further discussed here.

The strain rate sensitivity of the flow stress is chosen from Table 3.6. AISI 1045 is used for simulation, and Table 3.7 shows the material properties. Fig.3.8 shows the effect of strain rate sensitivity on plastic deformation under testing condition P=300MPa, Vcb=0.709m/s,μ=0.336.

3.2 Simulation result

The optimization of the temperature dependence of mechanical properties and the response function is then applied to the simulation model, and the simulation of

Table 3.6: Value of m

Category	Temperature	m
Cold working	$< 0.3T_m$	$0 - 0.05$
Warm working	$0.3T_m - 0.5T_m$	$0.05 - 0.1$
Hot working	$0.5T_m - 0.7T_m$	$0.05 - 0.4$

Table 3.7: Material properties of AISI 1045 steel

Density, ρ	7872 kg/m^3
Thermal conductivity, λ	49.8 $W/(m \cdot K)$
Specific heat, c	486 $J/(kg \cdot K)$
Shear modulus, G	80 GPa
Yield stress, σ	585MPa
Pressure, P	300MPa
Sliding velocity, V_{cb}	0.709 m/s
Friction coefficient μ	0.336

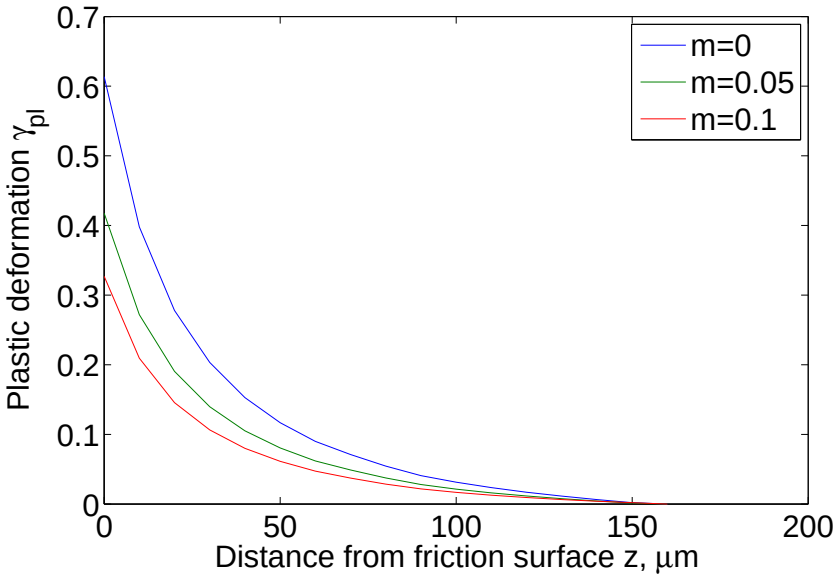

Figure 3.8: Effect of strain rate sensitivity on plastic deformation

Table 3.8: Simulation conditions for study of effect of contact duration

Density, ρ	7872 kg/m^3
Thermal conductivity, λ	49.8 $W/(m \cdot K)$
Specific heat, c	486 $J/(kg \cdot K)$
Shear modulus, G	80 GPa
Yield stress, σ	585MPa
Pressure, P	300MPa
Sliding velocity, V_{cb}	1 m/s
Friction coefficient μ	0.5

plastic deformation distribution of microasperity is studied.

Fig 3.9 shows the plastic deformation distribution of a microasperity after different sliding durations. With the increase of contact duration, the thickness and the degree of the plastic deformation of plastically deformed layers is increased. The reason for this phenomenon is that when the sliding time is increased, more heat is generated by friction on the friction surface. This heat will increase the temperature of the top layers of the microasperity and soften the material. Once the yield stress of the microasperity material decreases to a value below the shear stress, plastic deformation occurs.

Fig 3.10 shows the modification of the elastic property of the microasperity material. The relative maximum elastic deformation is the ratio of maximal elastic deformation under current conditions (thermal softened and work hardened), γ_{el}, and the normalized value of maximal elastic deformation, γ_{0el}. The normalized value means

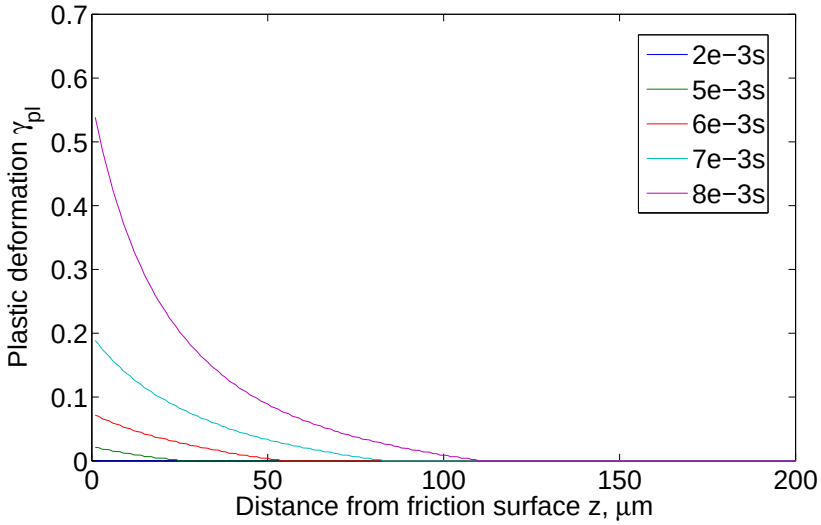

Figure 3.9: Effect of contact duration on plastic deformation

the value at 20°C before work hardening and thermal softening. Plastic deformation was occurred after certain contact duration, the maximum elastic deformation of plastically deformed layers is affected by both work hardening and thermal softening. The descending portions of the curves correspond to the hardened material and the ascending portions correspond to the softened material. The position of the minimum coincides with the thickness of plastically deformed layers.

3.3 Effect of testing conditions on plastic deformation

During the friction test, conditions such as contact pressure, sliding velocity, friction coefficient, temperature and humidity can affect the result significantly. Assuming that the temperature and humidity do not change during testing; the other three

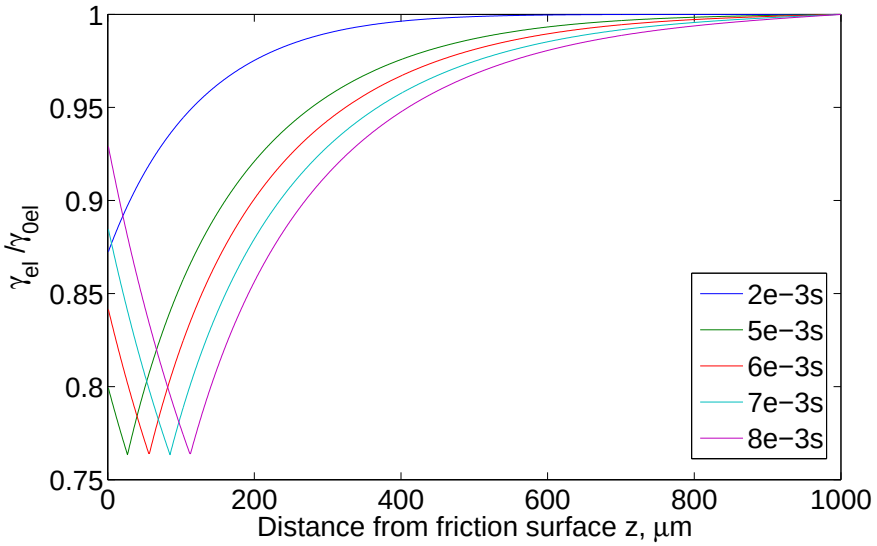

Figure 3.10: Effect of contact duration on relative maximal elastic deformation

factors will affect the energy input of testing specimens which will eventually affect the plastic deformation of the friction surface.

3.3 Effect of contact pressure

In the simulation, the process of softening of the material caused by friction heating is studied. Therefore, when specifying the initial conditions at the fixed friction coefficient and temperature, a value of contact pressure that can provide elastic deformation of the microaspetity at the initial moment and transition to plastic deformation when heated slightly was chosen.

$$\gamma_{0el} = \frac{\sqrt{\sigma^2 - P^2}}{\sqrt{3}G}, \quad \gamma = \frac{P\mu}{G} \tag{3.3.1}$$

When

$$\gamma_{0el} < \gamma$$

plastic deformation occurs. During the first moment of sliding, for only elastic deformation to happen at the friction surface, the following relationship has to be met.

$$P < \sqrt{\frac{\sigma^2}{3\mu^2 + 1}} \tag{3.3.2}$$

Table 3.9: Simulation conditions for study of effect of pressure

Density, ρ	7872 kg/m^3
Thermal conductivity, λ	49.8 $W/(m \cdot K)$
Specific heat, c	486 $J/(kg \cdot K)$
Shear modulus, G	80 GPa
Yield stress, σ	585MPa
Maximum plastic deformation, γ_{pl}^{max}	1
Sliding velocity, V_{cb}	1 m/s
Friction coefficient μ	0.5

Table 3.9 shows the simulation conditions used to study the effect of pressure. Fig 3.11 shows the effect of contact pressure on plastic deformation. For a single asperity, higher pressure means more energy input and it will take less time to reach a certain plastic deformation level.

3.3 Effect of counterbody velocity

Table 3.10 shows the simulation conditions used to study the effect of sliding velocity. Fig 3.12 shows the contact durations to reach a certain plastic deformation on the friction surface under different counterbody velocities. Fig 3.13 shows the effect

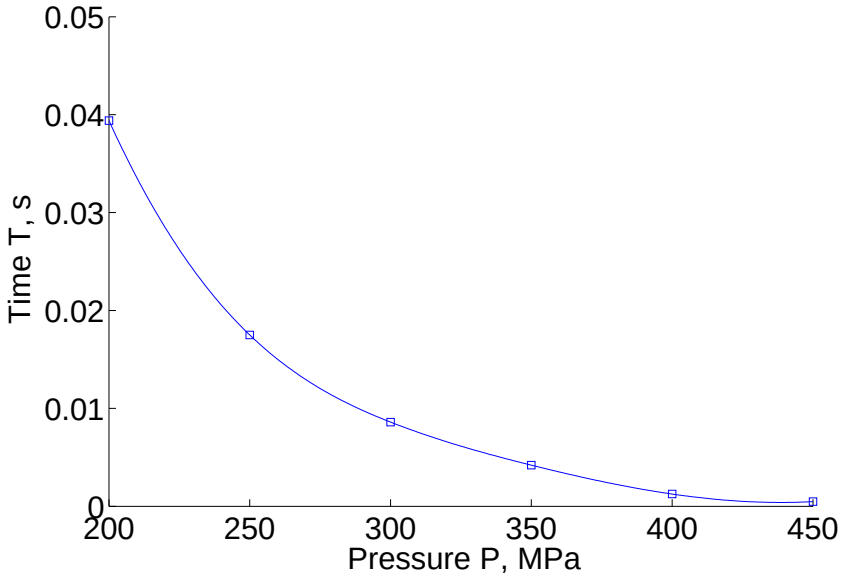

Figure 3.11: Effect of contact pressure on plastic deformation

of sliding velocity on deformed layers thickness. With shorter thermal conducting time, the thickness of the plastically deformed layers also decreased.

3.3 Effect of thermal conductivity on plastic deformation

Material properties affect the plastic deformation significantly, doing so directly, while the thermal properties of the material affect the thermal status and then affect the distribution of plastic deformation. The higher the thermal conductivity of the material the lower the temperature of the friction surface, which causes the lower degree of plastic deformation, and the lower temperature gradient (plastic deformation gradient) in the surface layers.

Table 3.10: Simulation conditions for study of effect of counterbody velocity

Density, ρ	7872 kg/m^3
Thermal conductivity, λ	49.8 $W/(m \cdot K)$
Specific heat, c	486 $J/(kg \cdot K)$
Shear modulus, G	80 GPa
Yield stress, σ	585MPa
Maximum plastic deformation, γ_{pl}^{max}	1
Pressure, P	300 MPa
Friction coefficient μ	0.5

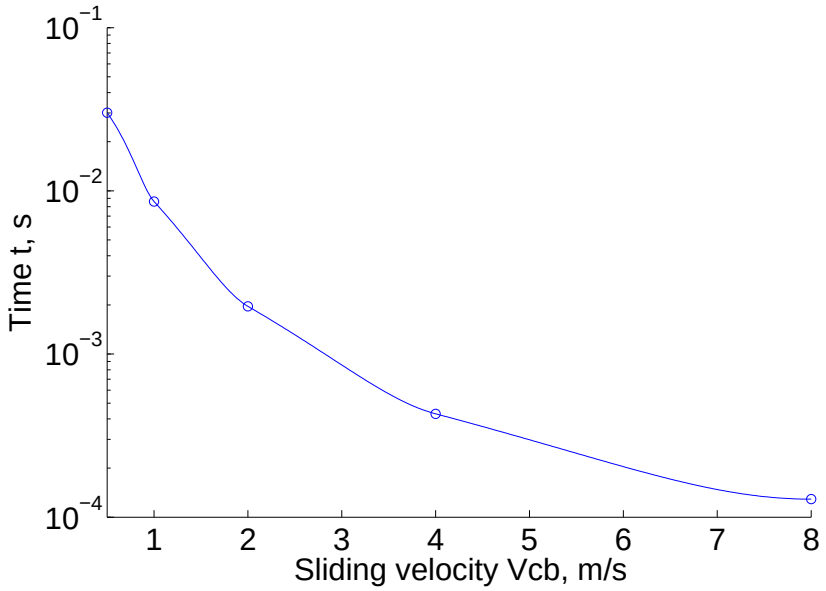

Figure 3.12: Effect of sliding velocity on contact duration

Table 3.11: Simulation conditions for study of effect of thermal conductivity

Density, ρ	7872 kg/m^3
Specific heat, c	486 $J/(kg \cdot K)$
Shear modulus, G	80 GPa
Yield stress, σ	585MPa
Maximum plastic deformation, γ_{pl}^{max}	1
Pressure, P	300 MPa
Sliding velocity, V_{cb}	1 m/s
Friction coefficient μ	0.5

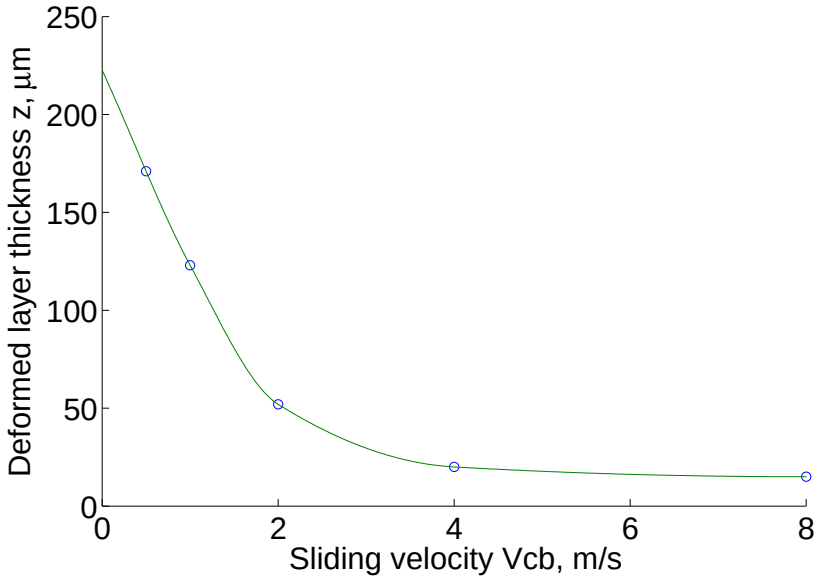

Figure 3.13: Effect of sliding velocity on deformed layer thickness

Fig 3.14 shows the effect of thermal conductivity on plastic deformed layer thickness. When reaching a certain plastic deformation on the friction surface, material having higher thermal conductivity will have a thicker deformed layer. The deformed layer thickness depends on the thermal conductivity non-monotonously.

3.4 Experimental validation of model

The model used to study plastic deformation under the friction surface was established. In order to validate the model, an experiment was designed. Several specimens were tested under different conditions using a pin-on-drum apparatus. The specimens were observed and the plastic deformation distribution under the friction surface were recorded. Multiple linear regression analysis is used here to find a best fit function

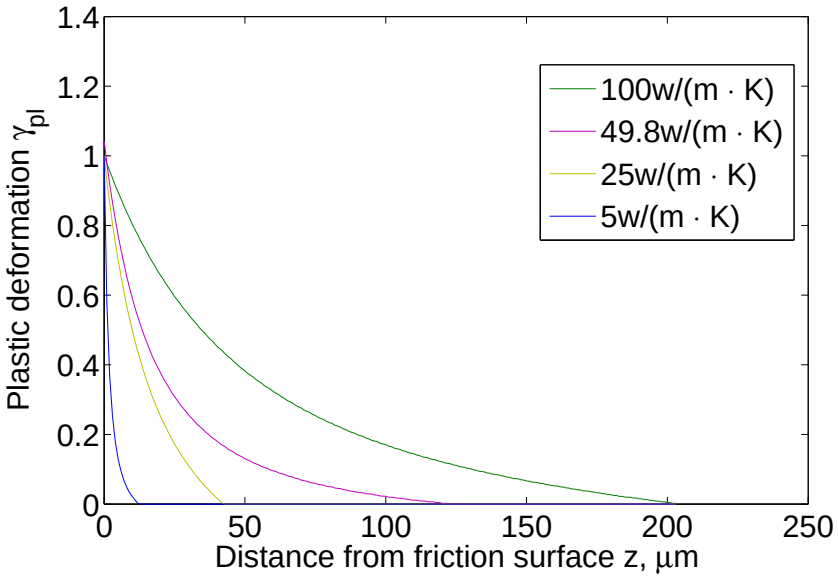

Figure 3.14: Effect of thermal conductivity on deformed layer thickness

which can be used as a description of the experimental data.

The simulation model will be run under testing condition to get a result to be compared with the testing data. F-value test is used to compare these two sets of data.

3.4 Experiment design

A pin on drum test was designed for the project. The pin on drum test is usually used to determine the wear resistance of a material when relative motion is caused between a abrasive counterbody and a contacting pin of the test material. The schematic diagram of the testing apparatus is shown in Fig 3.15. This test method

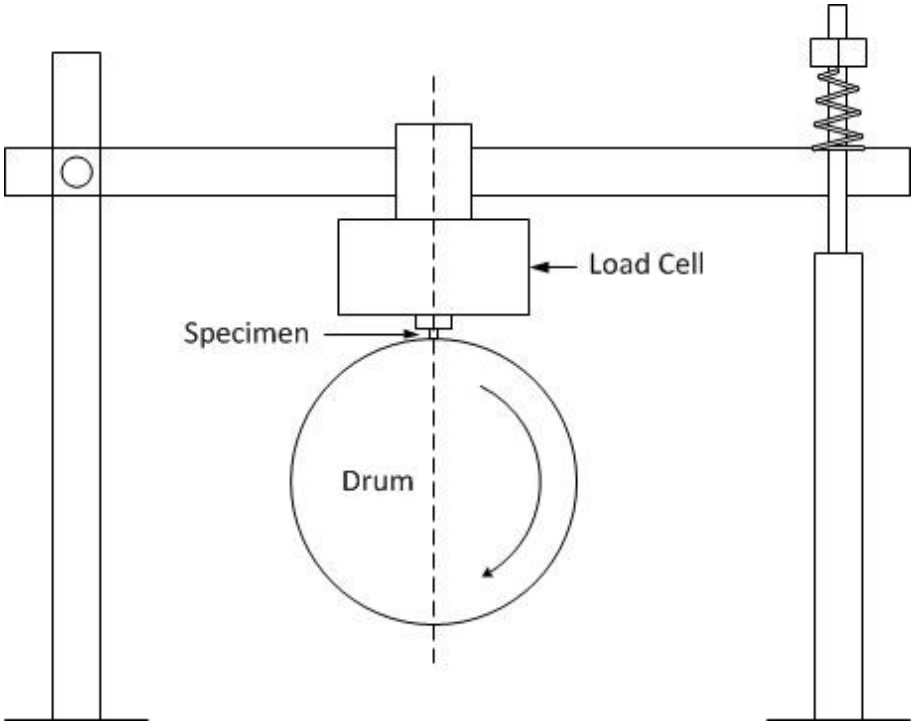

Figure 3.15: Schematic diagram of testing apparatus

involves a pin specimen that slides against the surface of a drum mounted on a lathe. The RPM and the sliding velocity are controlled using the setting of the lathe. The apparatus is shown in Fig 3.16.

The test method can be applied to different friction materials. The only requirement is that the specimens need to withstand the stresses imposed during the test without failure and excessive flexure. the specimens used in this project has AISI 1045 as the matrix material, which is strong enough to hold the pressure applied during test.

The standard of pin on drum test required that the reference material, which is

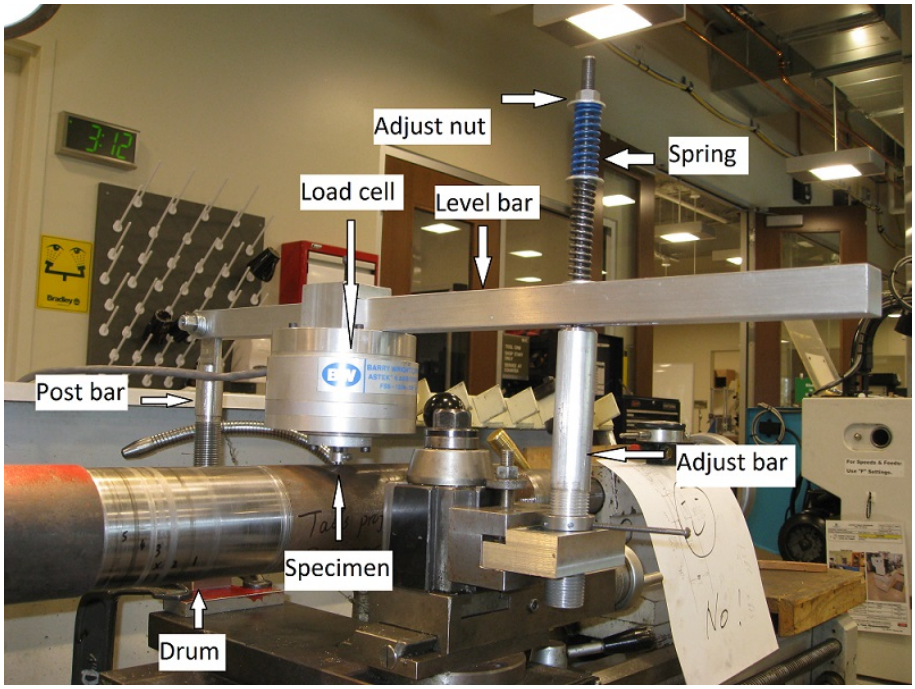

Figure 3.16: Apparatus of pin on drum test

Table 3.12: Chemical composition of AISI 4340 in weight percent

AISI No.	Fe	C	Mn	Si	Ni	Cr	Mo
4340	Balance	0.38/0.43	0.60/0.80	0.15/0.30	1.65/2.00	0.70/0.90	0.20/0.30

the counterbody in this dissertation, has a Brinell hardness of 269 or higher. And a surface roughness of 1 μm or less is adequate[53]. In this dissertation, the drum is made of normalized AISI 4340, which has a Brinell hardness of 363. In order to decrease the inter-lock effect between the drum and the specimen, the cylinder surface of the drum was grounded by using sand paper. The surface roughness is around 0.5 μm, which was measured by profilometer. Table 3.12 shows the Chemical composition of AISI 4340 in weight percent.

The apparatus contains three main parts which are the pin specimen, the drum and the load cell. The FS6-120A load cell, which is used to measure and record the load applied to the pin, is fixed on the horizontal level bar and the position is adjustable. The spring on the level bar is used to maintain the constant load on the pin by adjusting the nut on the top of the springs. The post bar is clamped on the carriage of the lathe, and the adjust bar is fixed on the tool post.

The frame of the apparatus need to be rigid, which means the during the friction test the post bar, level bar and adjust bar will not bend. Reason to do so is to restrict the position of specimen on the top center of the drum. The frame in this apparatus is made of aluminum which will slightly bend under the normal load and friction force during test. The bending is small compared to the diameter of the contact area of specimen and drum when equilibrium status is reached, so the assumption is made that the bending of frame is neglected.

Normal load and friction force was measured during friction test. and other force which is parallel to the the axis of drum is also detected by the load cell. It is because that the specimen is not perfectly perpendicular to the drum. The amplitude of the force is about 3N while the normal force is 100N and friction force is about 40N, so it could be ignored. After test, the load was recorded by load cell. Due to the vibration, the load is not a constant number at different time. The average normal force and average friction force was calculated.

Several things need to pay attention when set up a test. First, the specimen need to be centered on the top of drum. Second, the test should last long enough to make sure the specimen tip is fully contact withe the drum. This period usually take about 5 minutes. For the single material specimen, the orientation of the copper marker need to be perpendicular to the sliding direction.

The pin specimen used for the pin on drum test generally has a diameter range from 2 to 10 mm[53]. In order to measure the plastic deformation of the specimen surface, a special specimen which has a copper layer was prepared. A 12.7mm diameter rod of cold drawn AISI 1045 steel was bisected along its axis by diamond saw. The two semi-cylindrical pieces were brazed together, and then turned to a diameter of 5mm. The process of specimen preparation is shown in Fig 3.17. Fig 3.18a shows the cross-section of the specimen, and the area of red circle is shown in Fig 3.18b in microscopic scale.

The friction surface of the specimen was polished before testing in order to reduce the effect of surface roughness. The diameter of the drum and the RPM of the lathe are recorded before testing. The RPM of the lathe can be set to different values for different test conditions. The normal load applied on the pin can be read from the FS6-120A six-axis load cell. The counterbody velocity was calculated using the diameter of the drum and the RPM of lathe; normal pressure on the friction surface was calculated using the normal load applied on the pin and the dimension of the

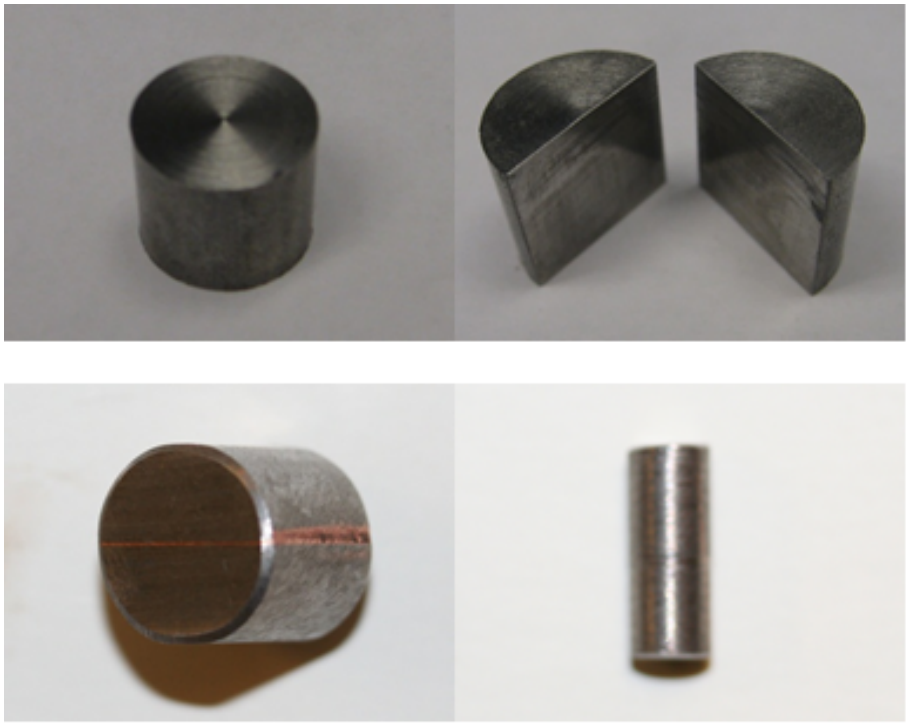

Figure 3.17: Preparation of specimen

pin. Friction force can be read from the load cell. These testing condition properties were put in the model to simulate the plastic deformation on the friction surface. The tested specimen was observed under microscope, and the actual plastic deformation was used to validate the model.

3.4 Actual plastic deformation distribution

The prepared specimens have been tested on the apparatus under different testing conditions which are listed in Table 3.13. D is the diameter of drum; RPM is the rotation rate of the drum; V is the linear speed between the drum and the specimen;

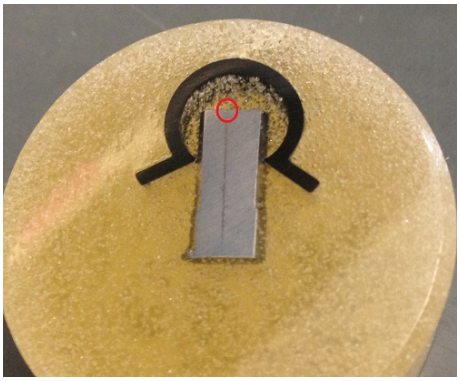

(a) Cross-section of specimen

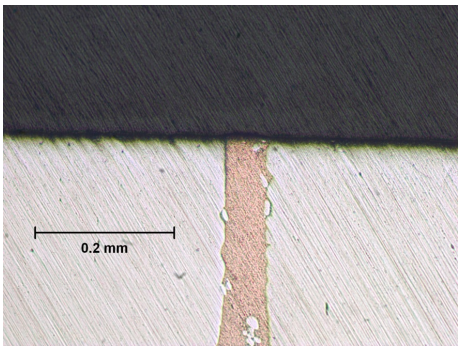

(b) Microscopic picture of cross-section

Figure 3.18: Cross-section of specimen

Table 3.13: Testing conditions

Testing No.	D (mm)	RPM (n/min)	v (m/s)	F (N)	μ	d (mm)	P (MPa)
0	79.7	90	0.376	46.4	0.494	5	2.363
1	79.7	90	0.376	51.2	0.662	5	2.608
2	79.7	90	0.376	67.7	0.507	5	3.448
3	79.7	90	0.376	73.6	0.478	5	3.748
4	79.7	130	0.709	52.8	0.436	5	2.689
5	79.7	130	0.709	83.4	0.421	5	4.248
6	79.7	130	0.709	105.4	0.591	5	5.368
7	79.7	170	0.709	46.4	0.433	5	2.363

F is the load applied on the specimen; d is the diameter of the specimen; A is the cross sectional area of the specimen; and P is the pressure applied on the specimen.

Afterward, test specimens were mounted in Lecoset 100 mounting resin, The specimens were ground flat, and the edges of the plastic beveled with a belt sander. The specimens are then hand ground using abrasive paper range from 240 through 600 grit. A single direction grinding stroke is used, and this direction is changed by 90° when going from one grinding paper to another. The specimens are washed between each

grinding step. The ground specimen is then polished with 1.0 μm alumina (Al_2O_3) on polishing wheel. Finally, the specimens are washed with water and methanol and then dried with a heat gun.

After polishing, specimens were observed under microscope, and pictures were taken (Fig 3.19). The red arrow shows the sliding direction of counterbody. The displacement of copper insert was measured(Fig 3.20). Measured testing results are present in following table 3.14.

Test 0 and test 1 have similar test conditions and their results were compared in Fig 3.21. The comparison shows that these results are very close, meaning the experiment is repeatable. The measured testing results were then plotted. For each test, the result is analyzed using multiple linear regression. Each group of test results can be fit with a exponential function, which can be used to describe the displacement of the copper insert under friction surface. Test results for specimens are listed below in Fig 3.22-3.28 with simulation results plotted in the same graph.

Simulation results are generated using the model and testing conditions. In order to make comparison between test results and simulation results convenient, the plastic shear calculated in the model is converted to displacement via equation 3.4.1:

$$x^k = \sum_{m=k}^{n} \gamma^m \cdot h_l \tag{3.4.1}$$

where x^k is the displacement of layer k, n is the total number of deformed layers, and h_l is the thickness of layers.

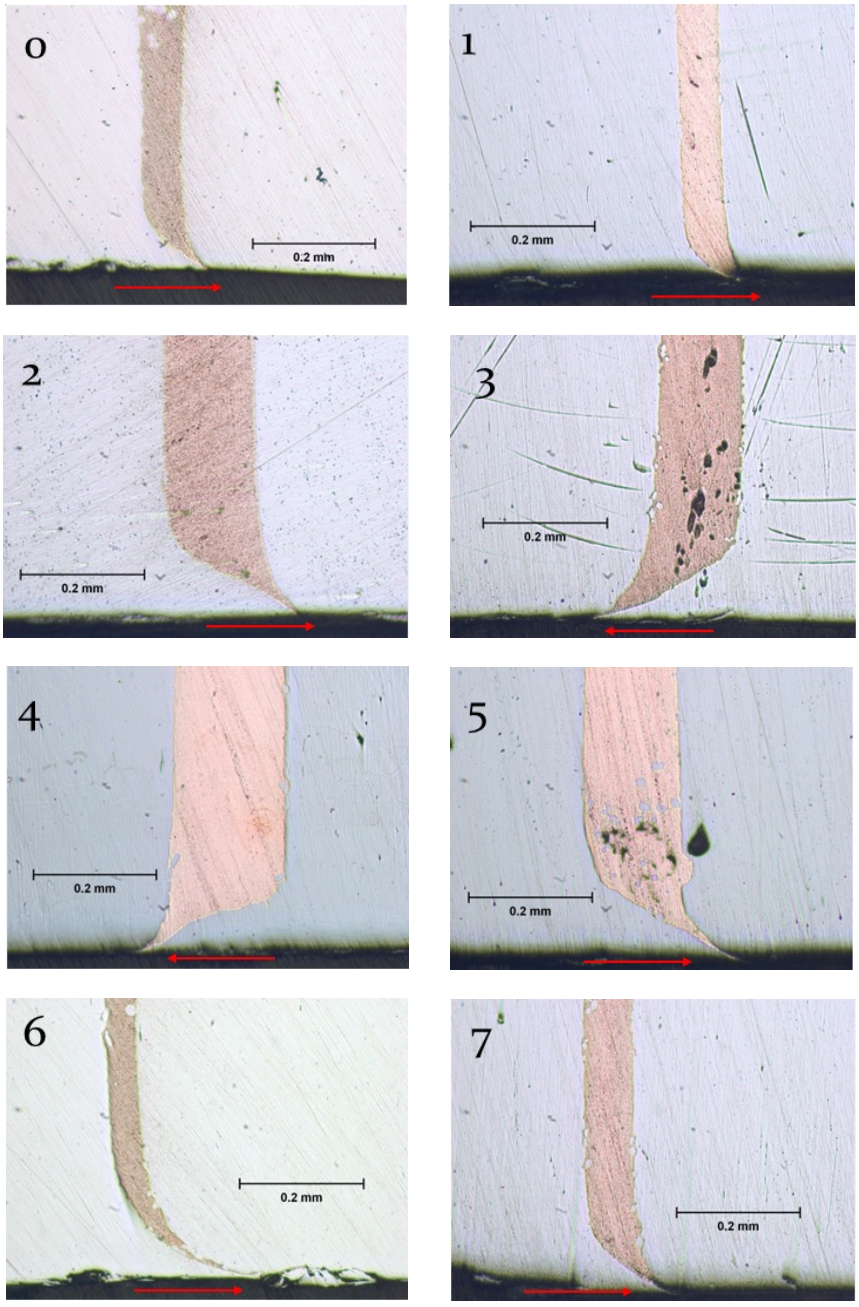

Figure 3.19: Microscopic pictures of specimens

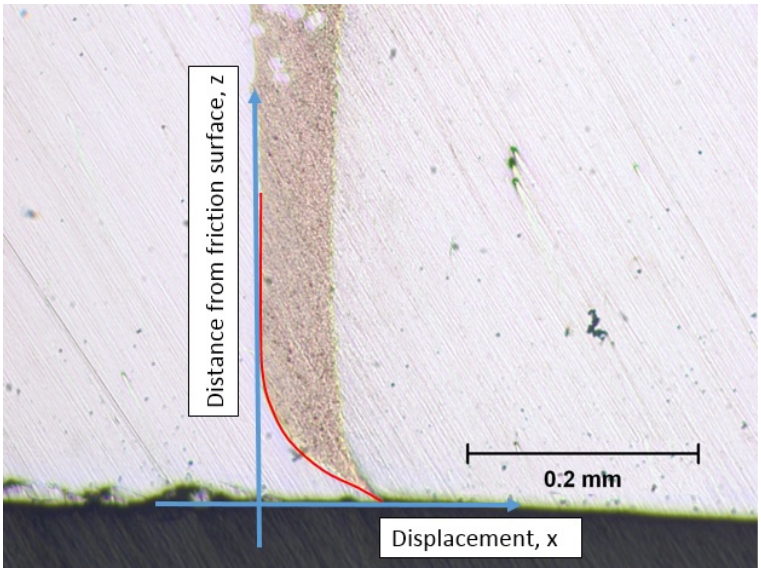

Figure 3.20: Measurement of plastic deformation

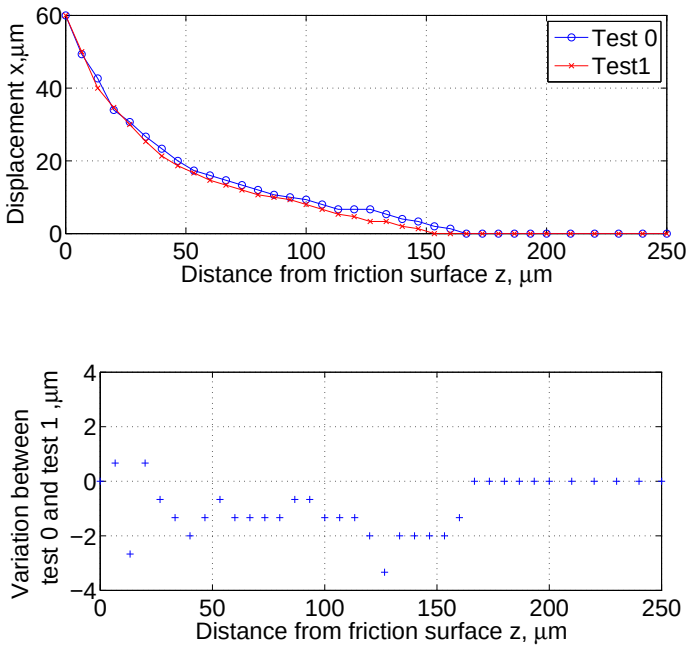

Figure 3.21: Comparison between test 0 and test 1

Table 3.14: Measured test results of specimens

Distance from friction surface z, μm	Displacement x, μm							
	Test 0	Test 1	Test 2	Test 3	Test 4	Test 5	Test 6	Test 7
0.0	60.0	60.0	63.3	83.3	60.0	86.7	93.3	80.0
6.7	49.3	50.0	59.3	70.0	46.7	70.0	80.0	56.7
13.3	42.7	40.0	53.3	63.3	40.0	56.7	66.7	40.0
20.0	34.0	34.7	46.7	57.3	30.0	50.0	53.3	32.0
26.7	30.7	30.0	40.0	53.3	23.3	43.3	46.7	26.7
33.3	26.7	25.3	35.3	48.7	18	36.7	43.3	22.0
40.0	23.3	21.3	30.7	43.3	14.7	30.0	40.0	17.3
46.7	20.0	18.7	26.7	38.7	11.3	24.7	33.3	15.3
53.3	17.3	16.7	23.3	34.7	10.3	18.7	28.0	13.3
60.0	16.0	14.7	21.3	30.7	6.7	13.3	28.0	11.3
66.7	14.7	13.3	20.0	27.3	5.3	8.7	24.7	10.7
73.3	13.3	12.0	16.7	25.3	3.3	5.3	21.3	10.0
80.0	12.0	10.7	16.0	23.3	2.7	3.3	20.0	8.7
86.7	10.7	10.0	13.3	20.0	1.3	2.0	16.7	6.7
93.3	10.0	9.3	11.3	18.7	0	0	15.3	6.7
100.0	9.3	8.0	10.7	16.7	0	0	14.0	5.3
106.7	8.0	6.7	10.0	15.3	0	0	13.3	3.3
113.3	6.7	5.3	8.0	13.3	0	0	11.3	2.0
120.0	6.7	4.7	6.7	12.0	0	0	10.0	0
126.7	6.7	3.3	6.0	10.0	0	0	8.7	0
133.3	5.3	3.3	5.3	8.0	0	0	7.3	0
140.0	4.0	2.0	3.3	6.7	0	0	6.0	0
146.7	3.3	1.3	1.3	4.7	0	0	4.7	0
153.3	2.0	0	0	4.0	0	0	2.7	0
160.0	1.3	0	0	2.0	0	0	1.3	0
166.7	0	0	0	0	0	0	0	0
173.3	0	0	0	0	0	0	0	0
180.0	0	0	0	0	0	0	0	0
186.7	0	0	0	0	0	0	0	0
193.3	0	0	0	0	0	0	0	0
200.0	0	0	0	0	0	0	0	0

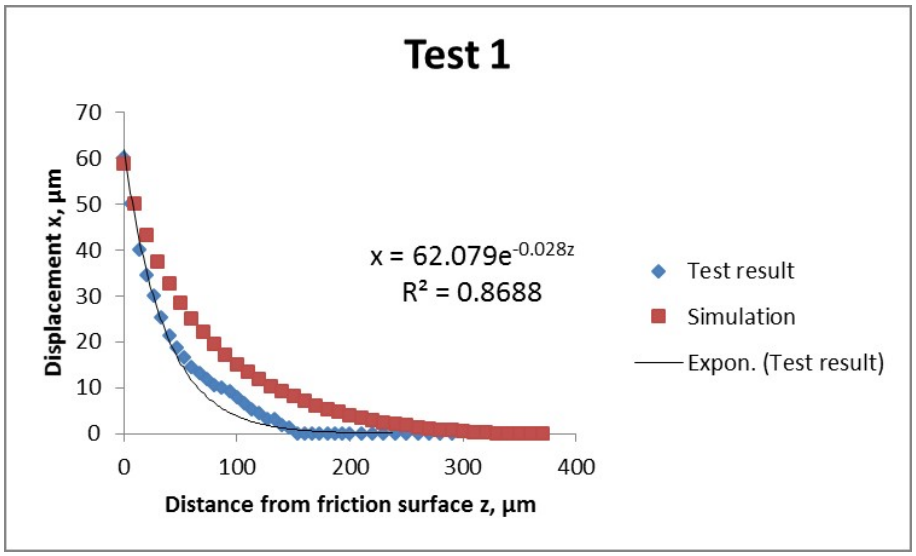

Figure 3.22: Result of test 1

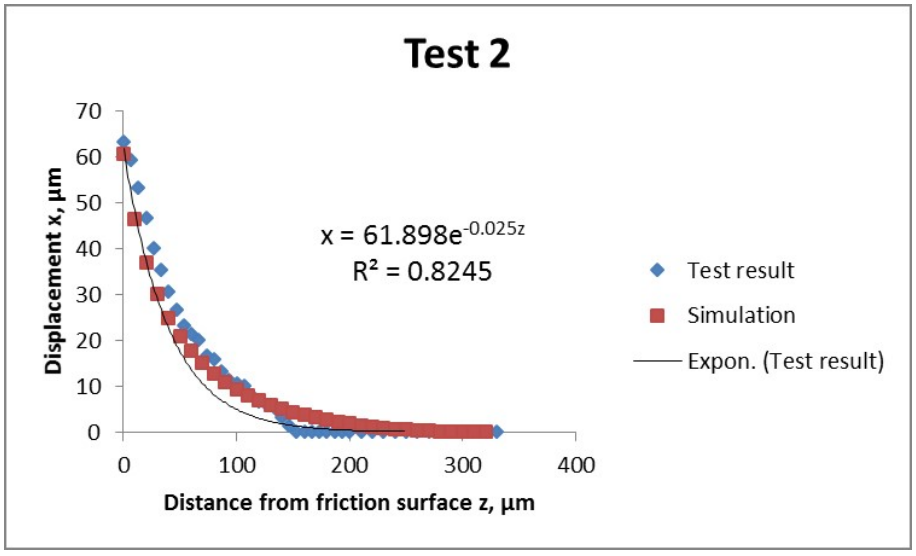

Figure 3.23: Result of test 2

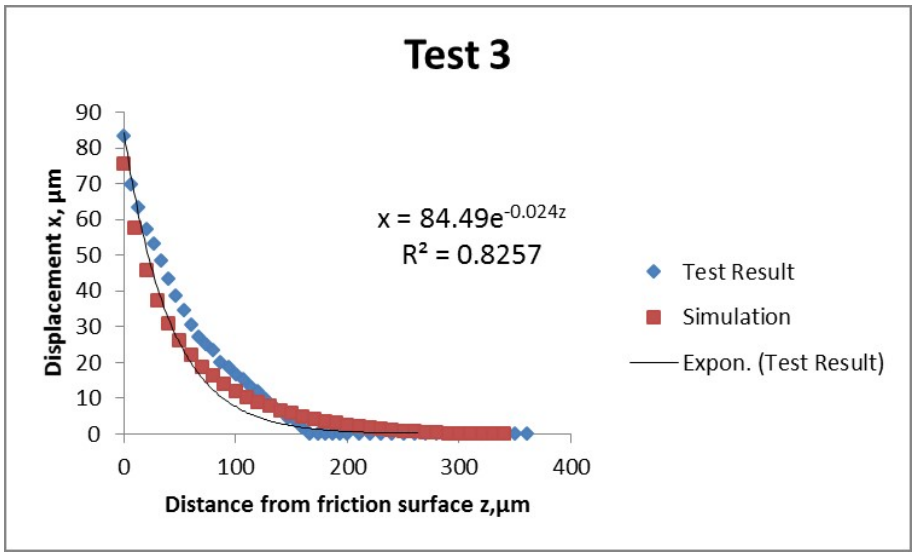

Figure 3.24: Result of test 3

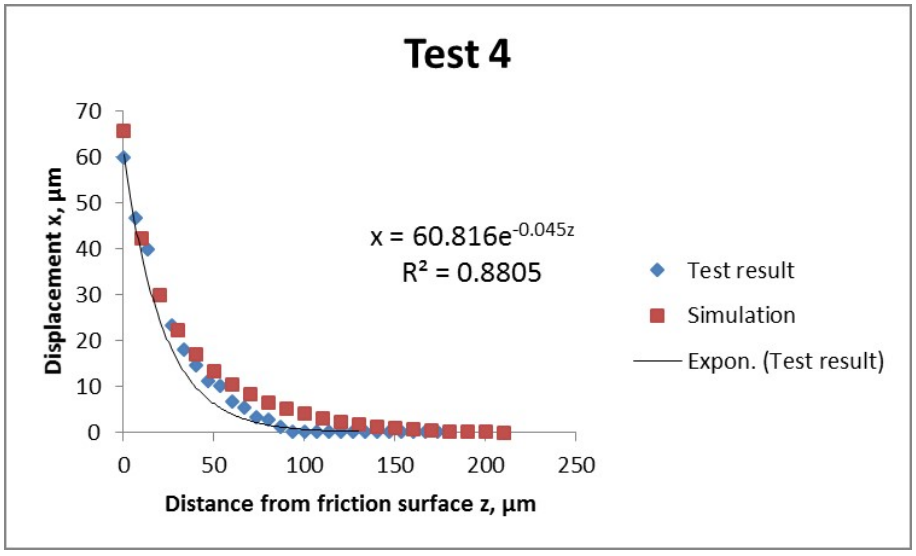

Figure 3.25: Result of test 4

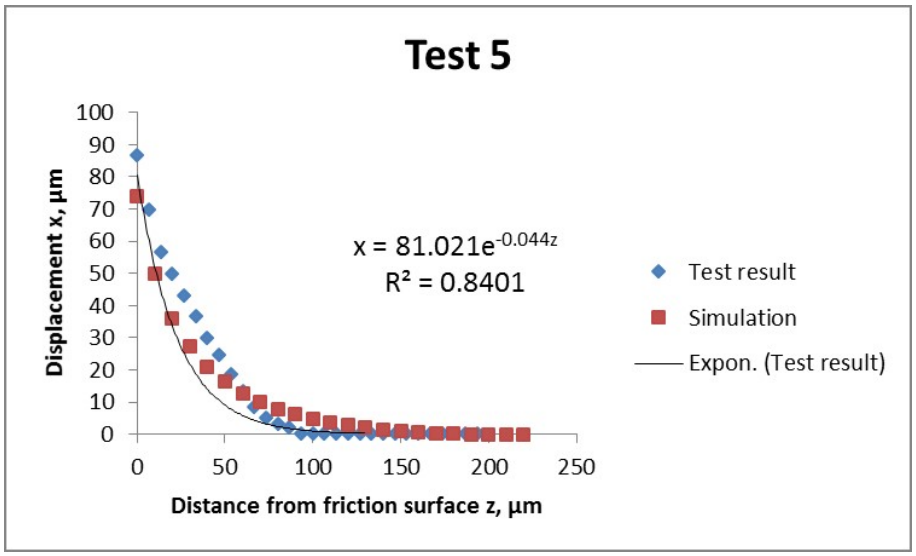

Figure 3.26: Result of test 5

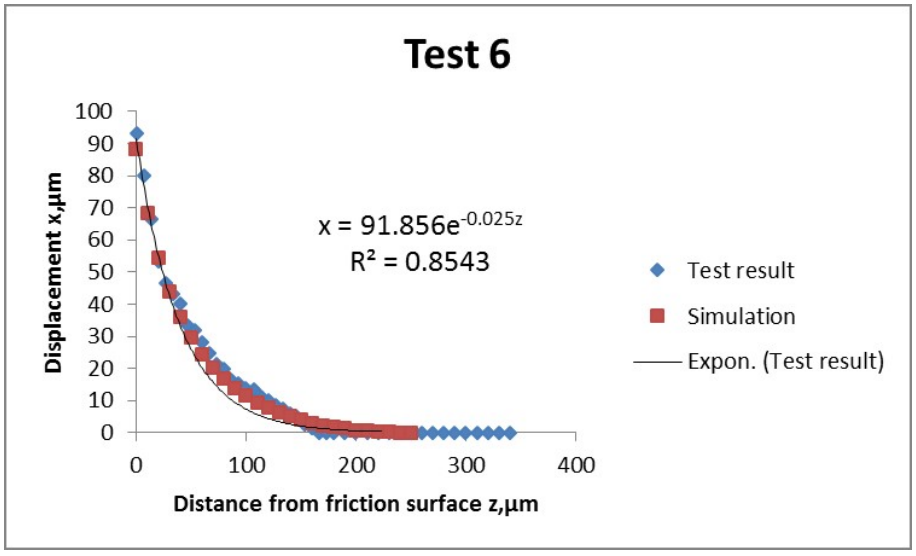

Figure 3.27: Result of test 6

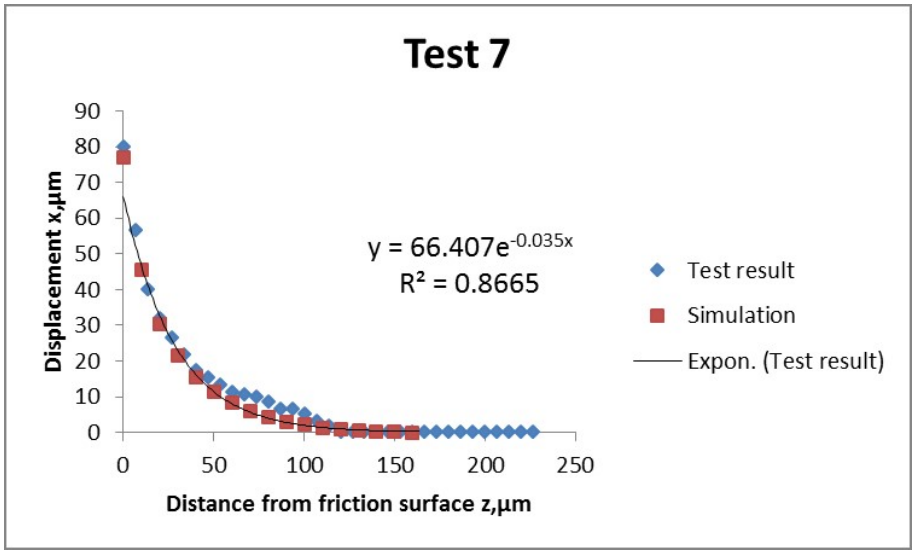

Figure 3.28: Result of test 7

In Fig 3.29, test results and simulation results having the same sliding speed were plotted together. With the increase of load, the displacement of the friction surface layer is increased, which validated the model.

In Fig 3.30, test results and simulation results having similar load but different sliding speeds were plotted together. With the increase of sliding speed, the displacement of layers near the friction surface is increased, which again validated the model.

3.4 Comparison of actual and simulated results

Variance analyses are approached for simulation results a test results. Tables 3.15 to 3.21 are the ANOVA table for test 1-7.

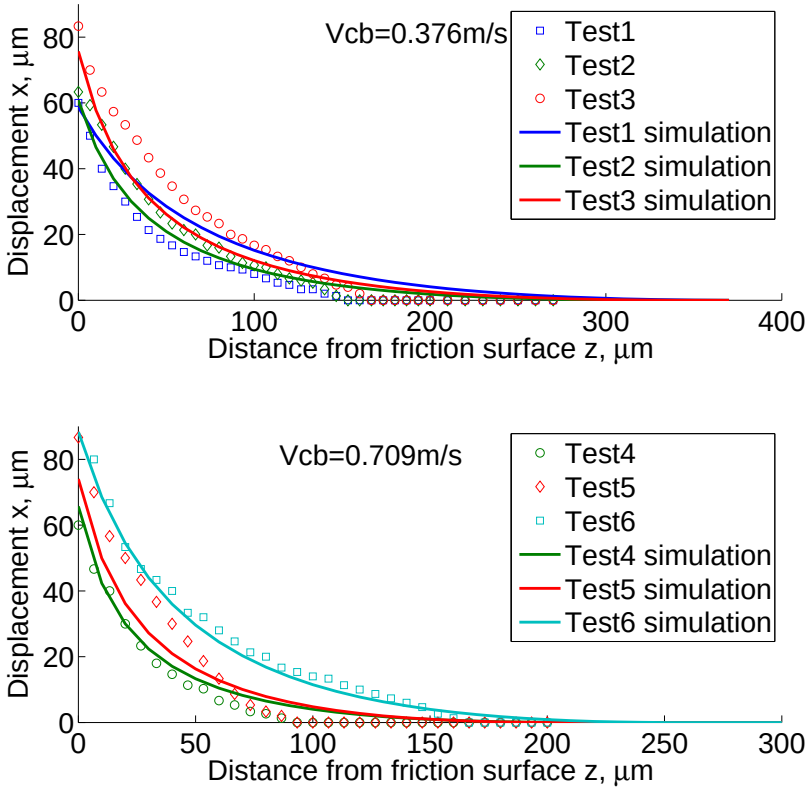

Figure 3.29: Effect of load on plastic deformation

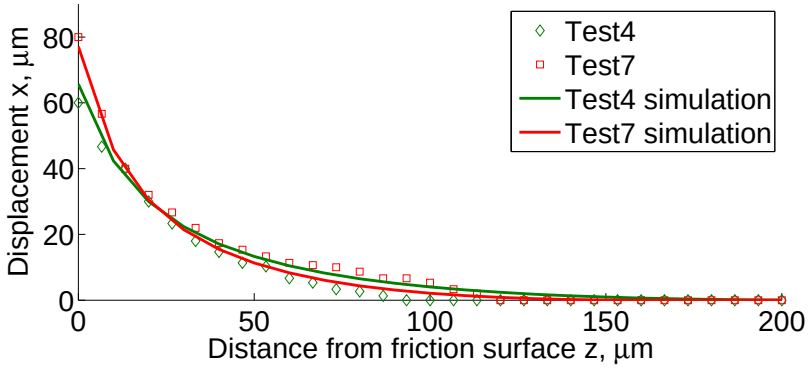

Figure 3.30: Effect of sliding speed on plastic deformation

Table 3.15: ANOVA of Test 1

Source of Variation	Sum of Squares	Degree of Freedom	Mean Square	Calculated f value
Regress	5175.2	1	5175.2	56.26
Residual	3403.6	37	91.99	
Total	8578.8	38		

Table 3.16: ANOVA of Test 2

Source of Variation	Sum of Squares	Degree of Freedom	Mean Square	Calculated f value
Regress	6402.8	1	6402.8	526.80
Residual	401.1	33	12.15	
Total	6803.9	34		

The calculated F-values are compared with critical values. If the calculated F-value is bigger than the critical F-value, the results are significant at the 5% significance level. One can conclude that there is strong evidence that the simulation results and the test results are similar. Table 3.22 is listing the F-value comparison.

3.5 Summary

In this chapter, a simulation model for plastic deformation under friction surface in a uniform material was established, and experiments were designed to validate the

Table 3.17: ANOVA of Test 3

Source of Variation	Sum of Squares	Degree of Freedom	Mean Square	Calculated f value
Regress	10429.3	1	10429.3	10203.5
Residual	37.8	37	1.02	
Total	10467.1	38		

Table 3.18: ANOVA of Test 4

Source of Variation	Sum of Squares	Degree of Freedom	Mean Square	Calculated f value
Regress	4540.8	1	4540.8	80.42
Residual	1185.6	21	56.46	
Total	5726.4	22		

Table 3.19: ANOVA of Test 5

Source of Variation	Sum of Squares	Degree of Freedom	Mean Square	Calculated f value
Regress	7626.6	1	7626.6	1138.95
Residual	147.3	22	6.70	
Total	7773.9	23		

Table 3.20: ANOVA of Test 6

Source of Variation	Sum of Squares	Degree of Freedom	Mean Square	Calculated f value
Regress	15552.5	1	15552.5	5734.62
Residual	92.2	34	2.712	
Total	15644.67	35		

Table 3.21: ANOVA of Test 7

Source of Variation	Sum of Squares	Degree of Freedom	Mean Square	Calculated f value
Regress	7015.1	1	7015.1	173.0
Residual	648.8	16	40.55	
Total	7663.8	17		

Table 3.22: F-value comparison

Test No.	$f_{0.05}(v_1, v_2)$	Calculated F-value
1	$f_{0.05}(1, 37) = 4.08$	56.26
2	$f_{0.05}(1, 33) = 4.17$	526.80
3	$f_{0.05}(1, 37) = 4.08$	10203.5
4	$f_{0.05}(1, 21) = 4.32$	80.42
5	$f_{0.05}(1, 22) = 4.30$	1138.95
6	$f_{0.05}(1, 34) = 4.17$	5734.62
7	$f_{0.05}(1, 16) = 4.49$	173.00

model. The model used testing conditions as inputs to predict the plastic deformation distribution under friction surface. The model can also be used to analyze the effects of different testing conditions making it useful in understanding the multi-factor friction process.

CHAPTER 4

Plastic Deformation Model for Composite with Single Additive Particle

Sintered metal based friction materials are used in clutches and brakes because of their superior mechanical and tribological properties. These materials have a metal matrix in which nonmetallic fibers, particles, and solid lubricants are dispersed. A variety of nonmetallic particles are added in different metal matrix forms to develop metal matrix composites.

Take copper based friction materials as an example, in order to achieve the required tribological properties, iron, SiO_2, MoS_2 and graphite are added to a copper matrix. Due to the different thermal and mechanical properties of these additives, the plastic deformation of the matrix metal, copper, will be different compared to uniform copper material. Depending on their purpose, additives can be divided into lubricating additives (MoS_2 and graphite), friction-abrasive additives (SiO_2) and reinforcement filler (iron). Their effects on plastic deformation of the matrix metal will be studied.

In this chapter, a model which has an additive particle in the matrix material is described.

4.1 Description of single additive composite model

Due to the complexity of friction materials, the plastic deformation analysis of a composite is studied using simple composite model under reasonable assumptions. A model which has an additive particle in the matrix material is described in Fig 4.1. The additive particle has its own thermal and mechanical properties which are different from the properties of the matrix material. The asperity is considered as a laminar structure, and each layer is assumed to be a rigid body. The counterbody is sliding on the top of asperity with velocity of V_{cb}. Heat is generated during the friction process and conducted to the asperity. Because of the difference in thermal properties, the matrix and additive materials in the same layer have different temperatures. In order to calculate the temperature distribution of the asperity, an assumption is made in which the matrix material and additive material can reach the same temperature via heat transfer.

A composite asperity has different plastic deformation behavior compared to that of a uniform material. The plastic deformation of the matrix metal is a function of mechanical and thermal properties, testing conditions and geometry of matrix metal and additive. Fig 4.2 show a schematic geometry of an additive particle. Each Particle could have a particular geometry function $Y(z)$.

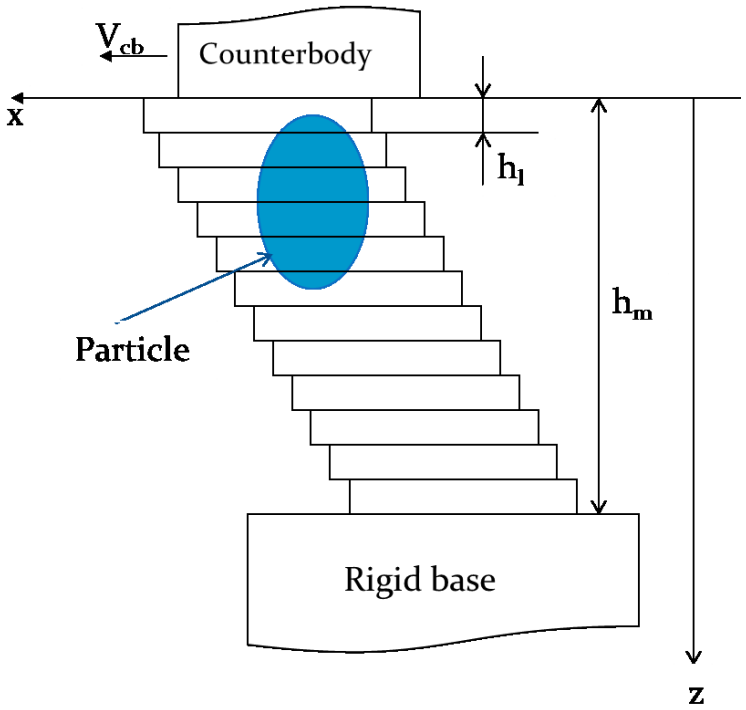

Figure 4.1: Composite model with one additive particle

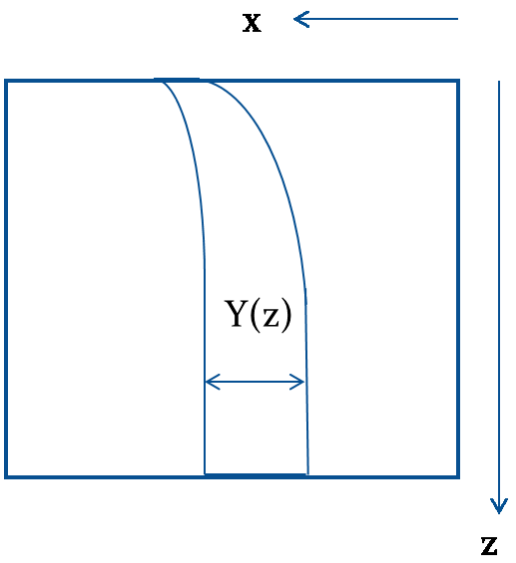

Figure 4.2: Geometry expression of additive particle

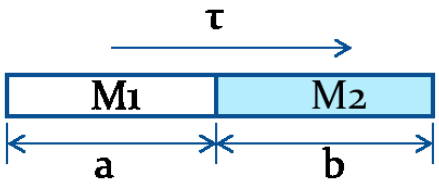

Figure 4.3: A layer from composite asperity

$$\gamma_{pl} = f\left(\sigma_m\left(T\right), G_m\left(T\right), \sigma_p\left(T\right), G_p\left(T\right), P, Y\left(z\right)\right)$$

$$T = g\left(P, V_{cb}, c, \lambda\right)$$

Fig 4.3 shows a one dimensional drawing of a layer from a composite asperity. M_1 and M_2 are two different materials; a and b are the lengths of M_1 and M_2 respectively. τ is the shear stress applied on this layer. Assuming that the layer is rigid; deformation is the displacement of the layer along the friction direction. The two materials will not separate during deformation and they will have same amount of deformation.

For elastic deformation:

$$\gamma_{el} = \frac{\left(a+b\right)\tau}{aG_1 + bG_2} = \frac{\tau}{\frac{aG_1+bG_2}{a+b}}$$

If the layer is of uniform material, then

$$\gamma_1 = \frac{\left(a+b\right)\tau}{aG_1 + bG_1} = \frac{\tau}{G_1}$$

$$\gamma \begin{cases} _{el} > \gamma_1 & G_1 > G_2 \\ \\ \gamma_{el} < \gamma_1 & G_1 > G_2 \end{cases}$$

For plastic deformation:

$$\gamma_1 = \gamma_2$$

γ_1 and γ_2 are the deformation of M_1 and M_2.

There are two situations that may occur. The first situation is only one material is plastically deformed, the other material is just elastically deformed.

$$\begin{aligned} \gamma_1 &= \gamma_{1,el} \\ \gamma_2 &= \gamma_{2,el} + \gamma_{2,pl} \end{aligned}$$

The second situation is when both M_1 and M_2 are plastically deformed.

$$\begin{aligned} \gamma_1 &= \gamma_{1,el} + \gamma_{1,pl} \\ \gamma_2 &= \gamma_{2,el} + \gamma_{2,pl} \end{aligned}$$

Equation 3.1.11 is modified to calculate the deformation for a composite asperity.

$$\gamma = \frac{\tau}{G'} + 0.002 \left(\frac{\tau}{\tau_y'} \right)^n$$

$G' = \frac{aG_1 + bG_2}{a+b}$, which can be considered as the shear modulus of the composite. and $\tau_y^{'}$ is the yield shear stress of the composite, which actually is the yield shear stress of the softer material.

Based on the analysis above, the plastic deformation of certain composite material layer can be calculated when the properties and length of both materials are known.

Material properties can be obtained from property test and handbook. The dimension of each material can be measured. In friction materials, the geometry of additives could be sphere, flake or irregular, which make the lengths of materials change in different layer. To decrease the amount of computation, special additive specimens are fabricated, in which the dimensions of matrix and additive material on each layer are about the same. The preparation of specimen is presented in the following section.

4.2 Preparation of specimen

Specimen with an additive particle has been prepared for friction tests. A 0.5 inch (12.7mm) long 0.2 inch (5mm) diameter cylinder is prepared first. The material used is AISI 1045 steel, which is the matrix material for the specimen. Then, a 0.0785 inch (1.99mm) diameter blind hole is drilled on the top of the cylinder, and the blind hole has a depth of 0.25 inch (6.35mm). The blind hole was filled by additive material for different additive effect studies. Fig 4.4 is a photo of a specimen. Fig 4.5 shows the dimension of matrix material specimen.

Specimens with copper, graphite and (SiO_2) were prepared. Copper brazing filler material (CDA 110), graphite rod and fused quartz rod are used to make these specimens. Table 4.1 is showing the properties of these additives.

Due to the limitation of quartz rod diameter, the blind hole dimension of the quartz additive specimen is different with that of copper and graphite specimens.

Figure 4.4: Matrix material specimen for composite model

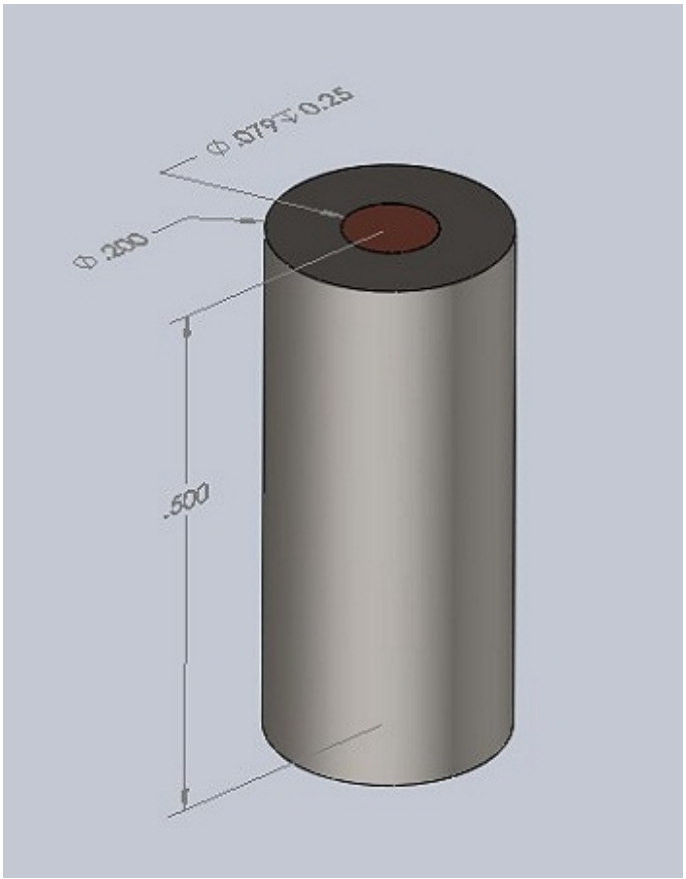

Figure 4.5: 3D model of the specimen

Table 4.1: Properties of additive materials

Material	ρ, kg/m^3	G, GPa	σ, MPa	λ, $W/(m \cdot K)$	c, $J/(kg \cdot K)$
AISI 1045	7872	80	585	49.8	486
Copper	8990	45.9	220	388	385
Graphite	1720	N/A	N/A	130	710
Quartz	2200	30.7	48	1.4	670

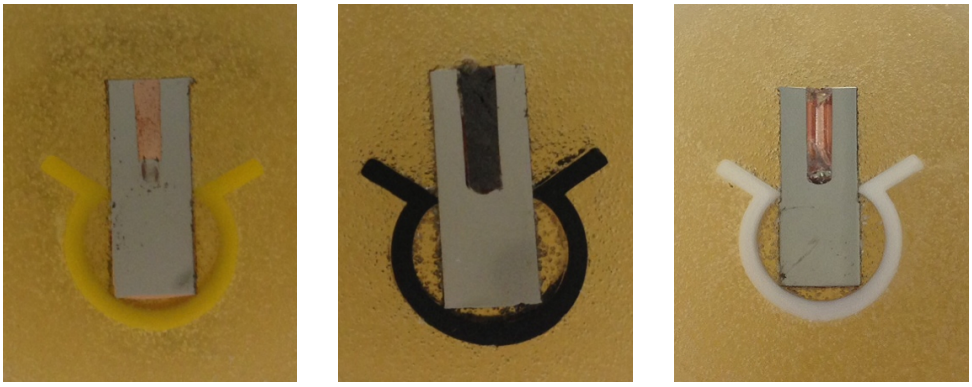

(a) Copper (b) Graphite (c) Quartz

Figure 4.6: Specimen with different additives

The quartz rod used in the experiment has a diameter of 0.0635in (1.61mm), so a No.51 drill, which has a diameter of 0.067in (1.7mm), was used.

For the copper additive specimen, a copper preform comprised of CDA110 copper, was placed on the top of specimen. The specimen was then placed in an atmosphere protected ($90\%N_2, 10\%H_2$) furnace at $1093°C$ ($2000°F$) and the copper preform melted and filled the blind hole. Graphite rod was cut down from a medium extruded grade GR060 graphite plate. Graphite rods and quartz rods were placed in the blind holes of specimens. Then, with some CDA110 on the top, these specimens

were heated in the atmosphere protected furnace to $1093°C$. The copper filler material melted and infiltrated into the gap between the additive particles and blind hole wall. A copper layer formed between the additive and the matrix metal, holding the additive in place. The thickness of the copper layer was very small compared to the dimension of the additive and matrix material, so its effect on deformation of matrix material was ignored. Fig 4.6 shows the actual see specimens.

4.3 Simulation of effect of copper additive on plastic deformation

Based on the analysis of composite model, the effect of copper additive on plastic deformation of matrix material under friction is simulated. The friction test results of copper additive composite specimen are used to compare to the simulation model.

4.3 Elevated temperature properties of CDA110

The thermal and mechanical properties of CDA110 as a function of temperature are presented in Table 4.2 [49, 54, 55]. Polynomial correlations of the yield strength as a function of temperature, using the data of Table 4.2 is as follows:

$$\sigma_{cu} = 199 + 0.382T - 0.00268T^2 \tag{4.3.1}$$

This equation is valid in the temperature range 293-1000K. Fig. 4.7 shows the variation of yield strength of pure copper with temperature.

Table 4.2: Variation of properties with temperature

T, K	λ, $W/(m \cdot K)$	c, $J/(kg \cdot K)$	σ_{cu}, MPa
293	400.68	383.48	210.74
300	401.00	385.00	210.00
350	396.78	392.00	206.52
373	395.20	394.73	205.00
400	393.00	398.44	205.00
450	389.93	403.00	197.81
473	388.35	405.90	195.00
500	386.50	408.00	181.50
550	383.08	412.00	156.74
573	381.50	414.80	140.00
600	379.00	417.00	126.48
650	376.23	421.00	94.83
673	374.65	422.42	85.00
700	372.80	425.00	85.00
773	367.80	429.76	35.00
800	366.00	432.00	26.32
873	360.96	437.82	10.00
900	359.11	441.00	
1000	352.00	451.00	
1073	347.26	460.07	
1100	345.41	464.00	
1200	339.00	480.00	
1250	335.13	490.00	
1300	331.71	506.00	

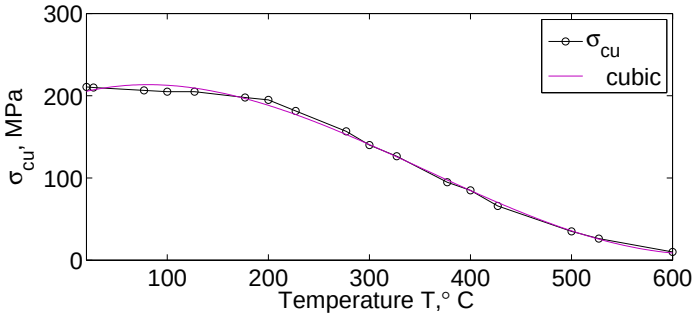

Figure 4.7: Yield strength of copper

Table 4.3: Testing conditions

Test No.	D (mm)	RPM (n/min)	v (m/s)	F (N)	μ	d (mm)	P (MPa)
c1	78.9	90	0.372	55.7	0.548	5	2.837
c2	78.9	90	0.372	73.6	0.503	5	3.748
c3	78.9	90	0.372	132.9	0.436	5	6.769
c4	78.9	130	0.537	45.7	0.462	5	2.327
c5	78.9	130	0.537	70.9	0.430	5	3.611
c6	78.9	130	0.537	120.9	0.475	5	6.157
c7	78.9	170	0.702	88	0.492	5	4.482

4.3 Friction test of copper additive composite specimens

The apparatus of the pin on drum test, which is shown in Fig 3.16 is used for the friction test of copper additive composite specimens. Test conditions are listed in Table 4.3. After test, the specimens are mounted, polished and observed with an optical microscope. Microscopic pictures of the specimens are taken, which are shown in Fig 4.8.

Specimens c1, c2 and c3 are tested under the same sliding speed but different load. Same as c4, c5 and c6. Test result of this two groups of specimen can be used to study the effect of load on plastic deformation. Test of specimen c2, c5 and c7 have similar load but different sliding speed, and test results of these three specimens can be used to study the effect of sliding speed on plastic deformation.

The measured testing results then are plotted. For each test, the result will be analyzed using Multiple Linear Regression. Each group of test result can generate a

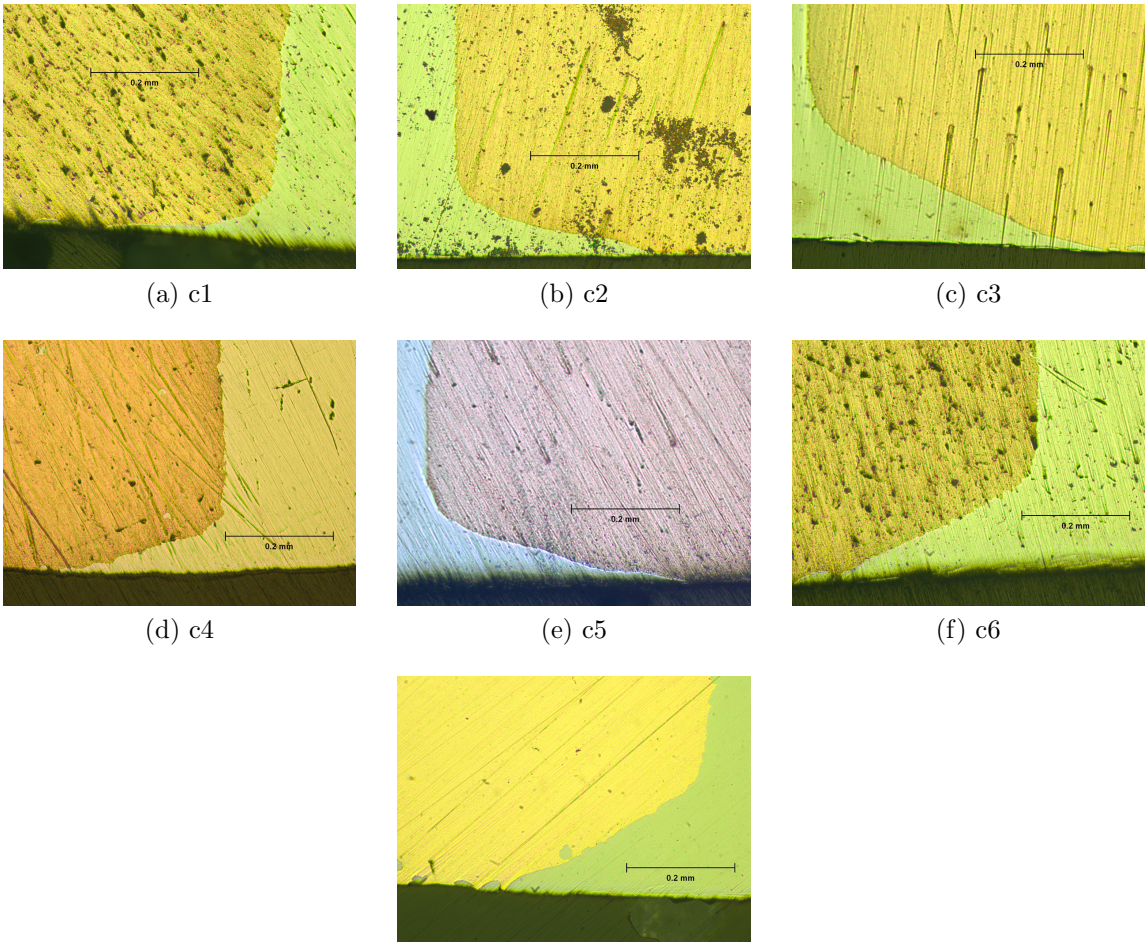

(a) c1 (b) c2 (c) c3

(d) c4 (e) c5 (f) c6

(g) c7

Figure 4.8: Microscopic pictures of copper additive specimens

Table 4.4: Measured test results of copper additive specimens

Distance from friction surface z, μm	Displacement x, μm						
	test c1	Test c2	Test c3	Test c4	Test c5	Test c6	Test c7
0	308.2	360.7	439.3	314.8	485.2	563.9	419.7
6.5	295.1	350.8	426.2	288.5	459.0	537.7	413.1
13.1	282.0	341.0	406.6	236.1	432.8	508.2	400.0
19.7	262.3	324.6	360.7	206.6	373.8	475.4	377.0
26.2	226.2	305.0	337.7	190.2	354.1	449.2	347.5
32.8	190.2	275.4	321.3	163.9	334.4	426.2	324.6
39.3	170.5	236.1	311.5	137.7	321.3	416.4	301.6
45.9	150.8	196.7	295.1	114.8	304.9	403.3	282.0
52.5	124.6	163.9	282.0	85.2	288.5	386.9	262.3
59.0	104.9	134.4	268.9	55.7	268.9	370.5	249.2
65.6	85.2	111.5	255.7	42.6	255.7	357.4	239.3
72.1	59.0	91.8	242.6	36.1	236.1	341.0	229.5
78.7	45.9	75.4	229.5	29.5	216.4	327.9	219.7
85.2	39.3	62.3	209.8	23.0	193.4	311.5	206.6
91.8	29.5	52.5	196.7	16.4	163.9	291.8	196.7
98.4	26.2	42.6	183.6	11.1	137.7	278.7	186.9
104.9	23.0	32.8	170.5	9.8	111.5	265.6	177.0
111.5	19.7	26.2	157.4	7.9	91.8	252.5	163.9
118.0	16.4	19.7	141.0	6.6	78.7	236.1	154.1
124.6	13.1	13.1	131.1	5.9	65.6	223.0	144.3
131.1	11.1	9.2	118.0	5.2	52.5	206.6	134.4
137.7	8.5	6.6	104.9	3.9	39.3	103.4	124.6
144.3	6.6	5.2	95.1	3.3	32.8	180.3	111.5
150.8	3.3	3.9	85.2	1.3	26.2	163.9	101.6
157.4	1.3	2.6	72.1	0	23.0	150.8	91.8
163.9	0	1.3	59.0	0	19.7	131.1	82.0
170.5	0	0	49.2	0	16.4	121.3	72.1
177.0	0	0	39.3	0	13.1	104.9	59.0
183.6	0	0	29.5	0	9.8	91.8	49.2
190.2	0	0	23.0	0	7.9	78.7	39.3
196.7	0	0	16.4	0	6.6	68.9	32.8
203.3	0	0	13.1	0	3.3	59.0	29.5
209.8	0	0	9.8	0	2.6	49.2	23.0
216.4	0	0	6.6	0	1.3	42.6	18.4
223.0	0	0	3.3	0	0	39.3	16.4
229.5	0	0	1.3	0	0	36.1	14.4

Table 4.5: Measured test results of copper additive specimens (continue)

Distance from friction surface z, μm	Displacement x, μm						
	test c1	Test c2	Test c3	Test c4	Test c5	Test c6	Test c7
236.1	0	0	0	0	0	29.5	13.1
242.6	0	0	0	0	0	26.2	11.8
249.2	0	0	0	0	0	23.0	11.1
255.7	0	0	0	0	0	21.0	9.8
262.3	0	0	0	0	0	18.4	8.5
268.9	0	0	0	0	0	15.1	7.9
275.4	0	0	0	0	0	13.1	7.2
282.0	0	0	0	0	0	11.1	6.6
288.5	0	0	0	0	0	9.8	5.2
295.1	0	0	0	0	0	7.9	4.5
301.6	0	0	0	0	0	6.6	3.3
308.2	0	0	0	0	0	4.6	2.6
314.8	0	0	0	0	0	2.6	1.3
321.3	0	0	0	0	0	1.3	0
327.9	0	0	0	0	0	0	0

exponential function which can be used to describe the displacement of the matrix material under the friction surface. Test results for specimen are listed below in fig 4.9-4.15. And simulation results are plotted on the same graphs.

In Fig 4.16, test results and simulation results that have the same sliding speed were plotted together. With the increase of load the displacement of friction surface layer is increased, which validated the model.

In Fig 4.17, test results and simulation results that have similar load but have different sliding speed were plotted together. With the increase of sliding speed the displacement of layers near friction surface is increased, which evidenced the model.

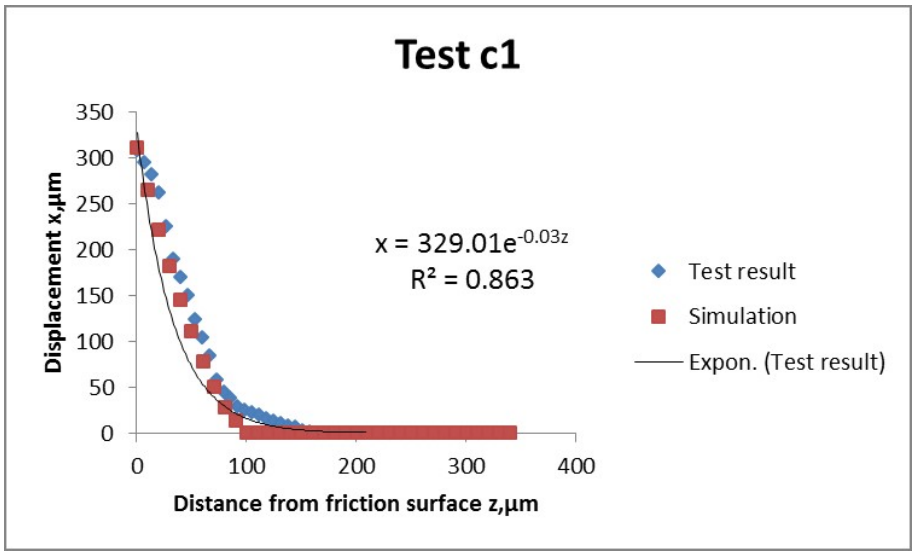

Figure 4.9: Result of test c1

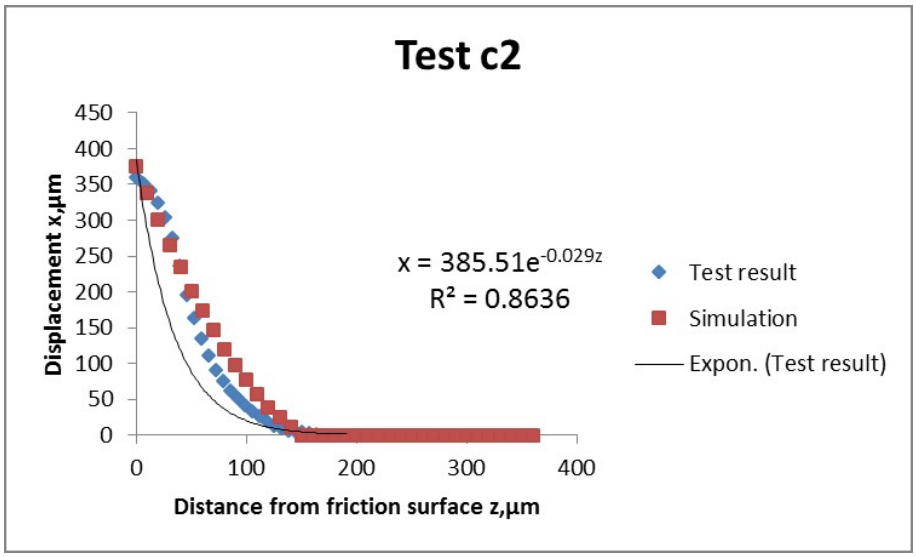

Figure 4.10: Result of test c2

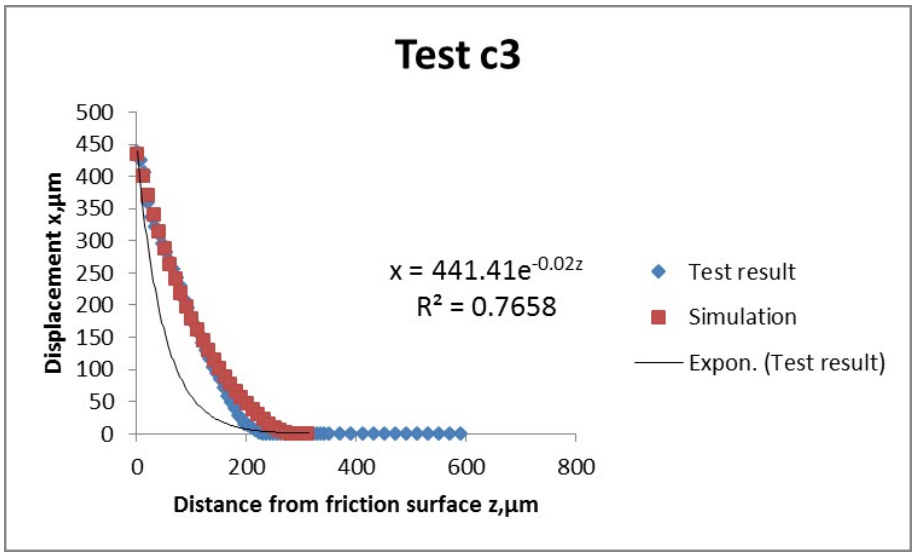

Figure 4.11: Result of test c3

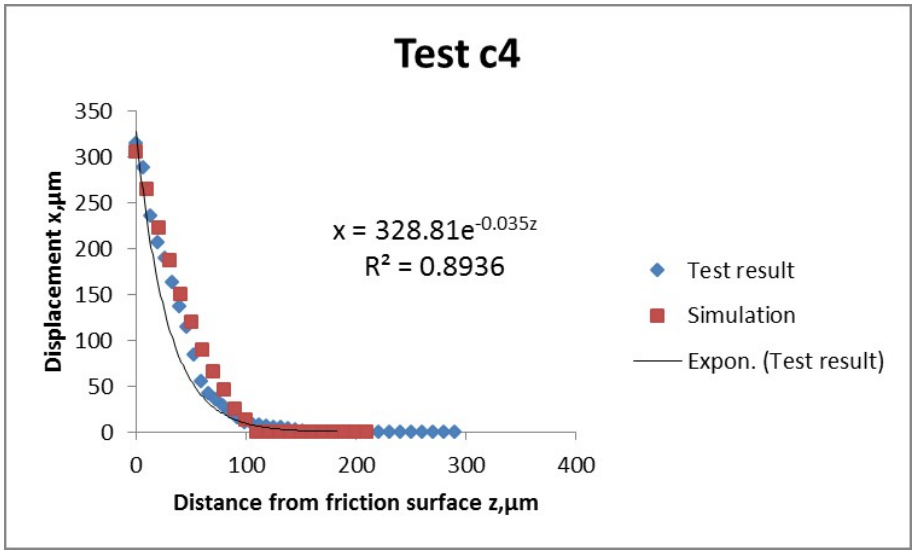

Figure 4.12: Result of test c4

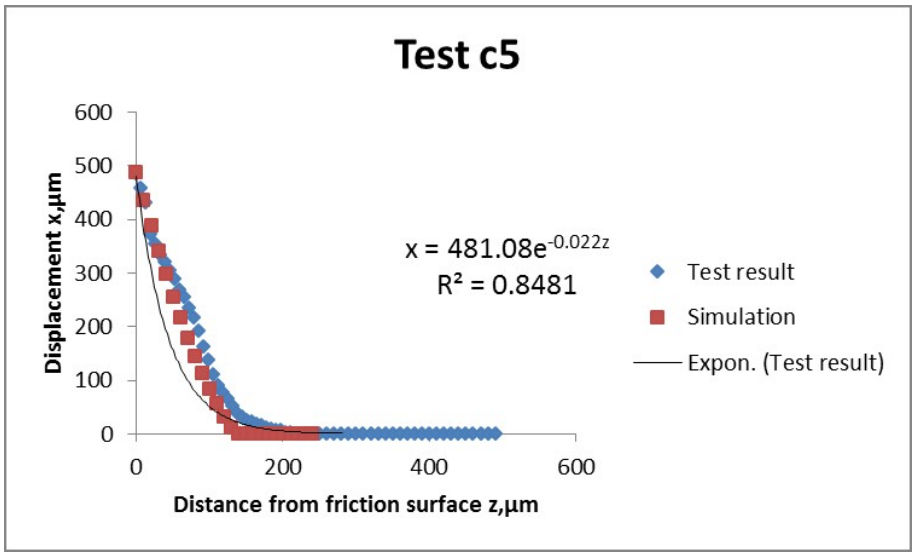

Figure 4.13: Result of test c5

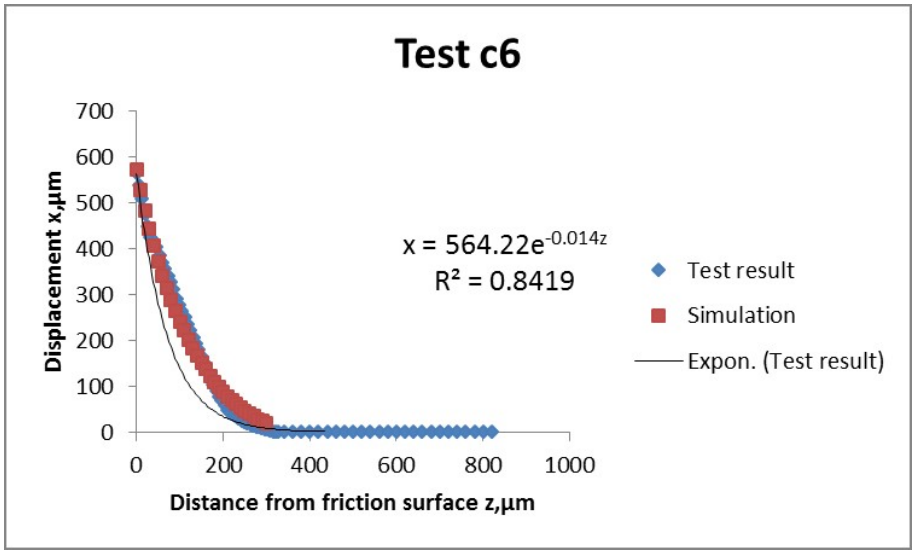

Figure 4.14: Result of test c6

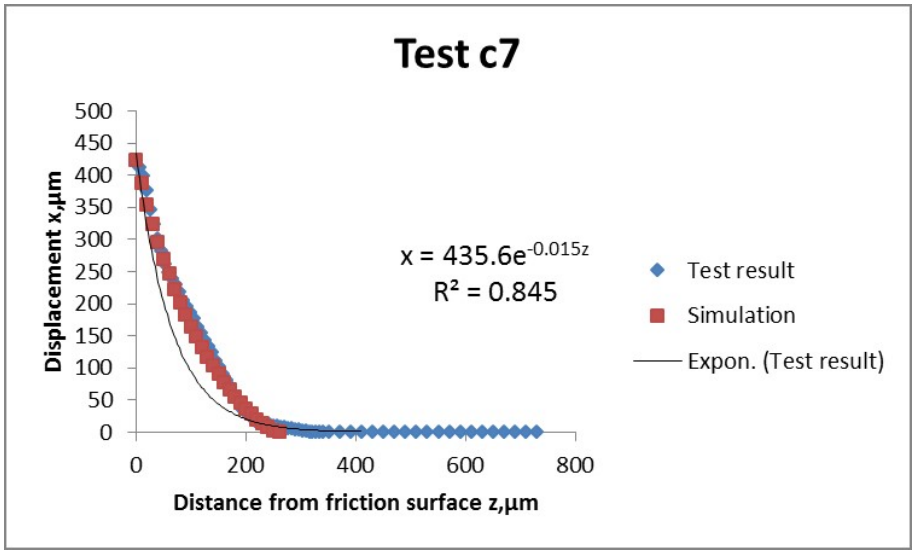

Figure 4.15: Result of test c7

Table 4.6: ANOVA of Test c1

Source of Variation	Sum of Squares	Degree of Freedom	Mean Square	Calculated f value
Regress	81243.1	1	81243.1	41.25
Residual	31514.2	16	1969.64	
Total	112757.3	17		

Variance analyses are approached for simulation results to multiple regression function of test results. Tables 4.6 to 4.12 are the ANOVA table for test c1-c7.

The calculated F-values are compared with critical values. If calculated F-value is bigger than critical F-value, the results are significant at the 5% significance level. One can conclude that there is strong evidence that the simulation results and the test results are similar. Table 4.13 is the list of the F-value comparison.

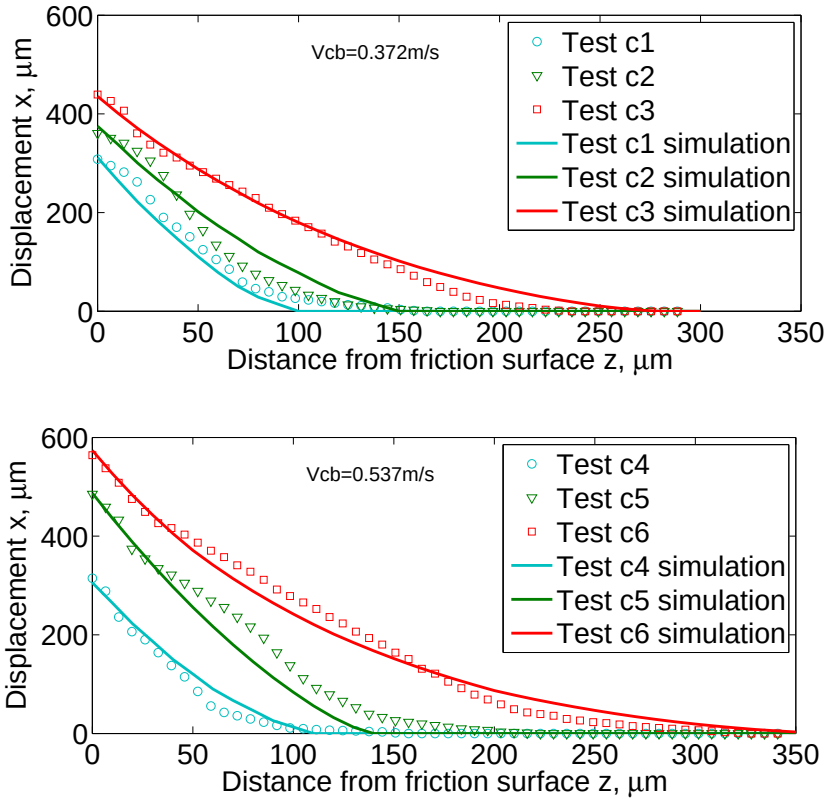

Figure 4.16: Effect of load on plastic deformation

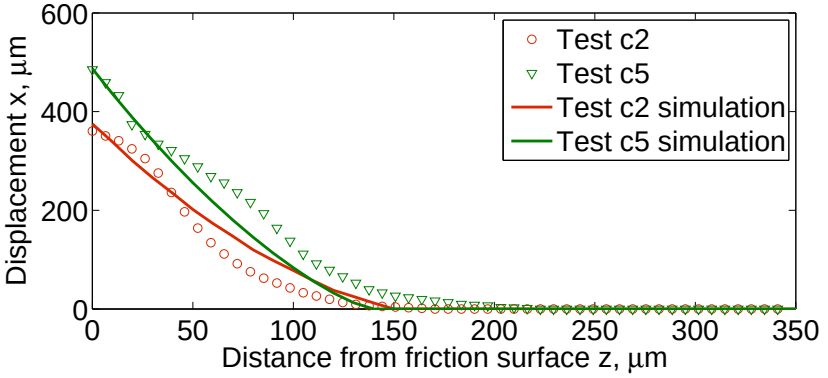

Figure 4.17: Effect of sliding speed on plastic deformation

Table 4.7: ANOVA of Test c2

Source of Variation	Sum of Squares	Degree of Freedom	Mean Square	Calculated f value
Regress	242932	1	242932	50.64
Residual	172700	36	4797.22	
Total	415632	37		

Table 4.8: ANOVA of Test c3

Source of Variation	Sum of Squares	Degree of Freedom	Mean Square	Calculated f value
Regress	316852	1	316852	23.58
Residual	376264.7	28	13438.03	
Total	693116.7	29		

Table 4.9: ANOVA of Test c4

Source of Variation	Sum of Squares	Degree of Freedom	Mean Square	Calculated f value
Regress	145388	1	145388	29.13
Residual	54904.9	11	4991.35	
Total	200292.9	12		

Table 4.10: ANOVA of Test c5

Source of Variation	Sum of Squares	Degree of Freedom	Mean Square	Calculated f value
Regress	163831.3	1	163831.3	12.02
Residual	190840.7	14	13631.48	
Total	354672	15		

Table 4.11: ANOVA of Test c6

Source of Variation	Sum of Squares	Degree of Freedom	Mean Square	Calculated f value
Regress	888210.8	1	888210.8	75.61
Residual	434672.4	37	11747.7	
Total	1322883	38		

Table 4.12: ANOVA of Test c7

Source of Variation	Sum of Squares	Degree of Freedom	Mean Square	Calculated f value
Regress	51443.1	1	51443.1	76.77
Residual	174237.3	26	6701.44	
Total	688680.4	27		

Table 4.13: F-value comparison

Test No.	$f_{0.05}(v_1, v_2)$	Calculated F-value
c1	$f_{0.05}(1, 16) = 4.49$	41.25
c2	$f_{0.05}(1, 36) = 4.08$	50.64
c3	$f_{0.05}(1, 28) = 4.20$	23.58
c4	$f_{0.05}(1, 11) = 4.84$	29.13
c5	$f_{0.05}(1, 14) = 4.60$	12.02
c6	$f_{0.05}(1, 37) = 4.08$	75.61
c7	$f_{0.05}(1, 26) = 4.23$	76.77

4.4 Simulation of the effect of lubricant additive on plastic deformation

Lubricant is a very important additive of friction materials. It can help to maintain a stable friction coefficient and keep a lower wear rate. The most common lubricant used in friction materials is graphite, which is easy to obtain, inexpensive, and can handle relatively high temperature and pressures. In this part of the project, the effect of graphite on plastic deformation of the matrix material during friction sliding will be discussed.

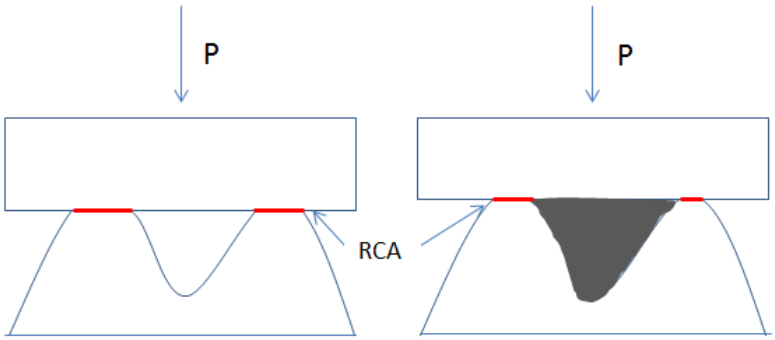

Figure 4.18: Effect of graphite on RCA

4.4 Effect of graphite on real contact area

In the research of wear behaviour of copper-graphite brushes, Yasar [56] and his co-workers found that graphite particles reduce the metal-to-metal contact area,which results in lower friction coefficients. Their SEM photograph also shows that the real contact area is relatively small. The schematic 4.18 shows the RCA with and without graphite under similar pressure. Although the SEM results of Yasar's research explained the effect of graphite on real contact area, the detailed relationship between graphite and real contact area is still unclear. Because the effect of graphite on RCA is not the emphases of this project, an reasonable assumption will be made on the amount of RCA when simulate lubricant additive model.

4.4 Effect of graphite on temperature distribution of asperity

The properties of graphite is listed in Table 4.1. A model similar to the copper additive model is used to simulate the temperature distribution of graphite additive asperity. Table 4.14 shows the simulation condition.

Table 4.14: Testing conditions of graphite additive sample

D (mm)	RPM (n/min)	v (m/s)	F (N)	μ	d (mm)	P (MPa)
78	90	0.368	43.9	0.143	5	2.236

The measured friction coefficient of the graphite additive sample is 0.143, which is much lower than that of the iron sample. The friction coefficient of the iron samples are about 0.5, which are shown in Table 3.13. This is a consequence of the lubricating nature and layered structure of graphite. Comparison of the temperature distribution between samples with and without graphite additive is presented in Fig 4.19. Besides the light weight, both thermal conductivity and specific heat capacity of graphite is higher than iron, which make the effect of graphite on temperature distribution is not significant.

4.4 Effect of graphite on plastic deformation

Based on the simulation of the temperature distribution of the graphite additive model, plastic deformation was analyzed. The conditions for the tests ares listed in Table 4.14. The cross-section of tested graphite additive sample is shown in Fig 4.20.

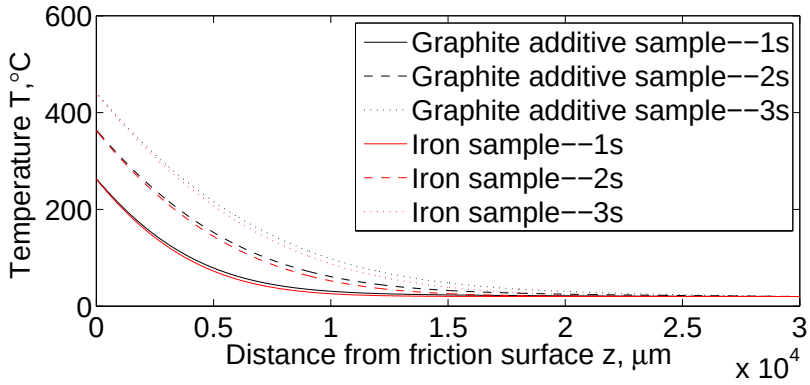

Figure 4.19: Microscopic pictures of graphite additive specimens

Table 4.15: ANOVA of Graphite additive sample Test result

Source of Variation	Sum of Squares	Degree of Freedom	Mean Square	Calculated f value	p
Regress	337.1	1	337.133	0.63	0.4311
Residual	18056.8	34	531.081		
Total	18393.9	35			

The test results of iron-graphite sample and simulation are plotted in Fig 4.21.

4.4 Summary of effect of graphite

The plastic deformation of an iron sample under the same test conditions is potted with that of graphite additive sample in Fig 4.22. Based upon the comparison of the two results, the effects of graphite additive are discussed.

The first difference between these two results is that the thickness of plastically deformed layer of the graphite additive sample is smaller than that of the iron sample.

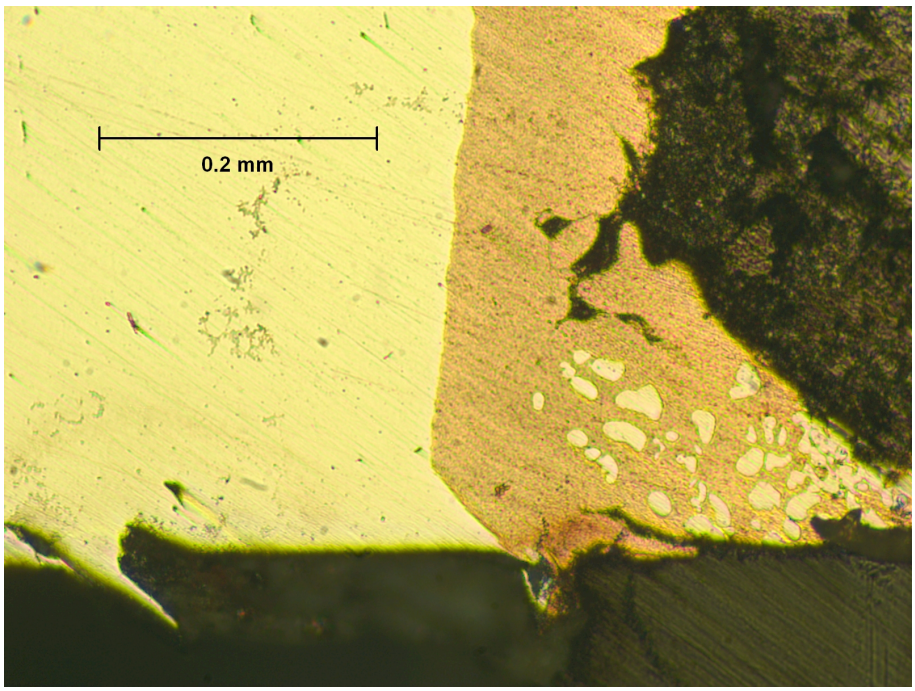

Figure 4.20: Microscopic pictures of graphite additive specimens

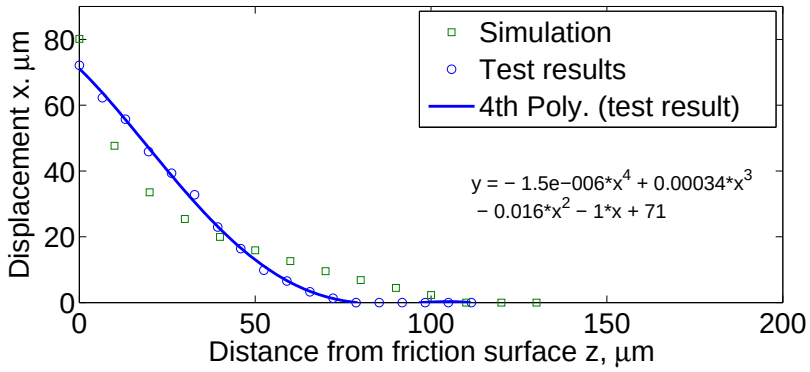

Figure 4.21: Effect of graphite on plastic deformation of matrix material

The deformation results were obtained after a period of time long enough for the run-in process to occur. Therefore the data collected is that of the equilibrium state. Due to the appearance of graphite, the friction coefficient is dropped significantly, which will also reduce the energy input to the friction material. Along with the thermal conduction and thermal convection, the energy flow into and out of the friction material will reach a balance point, which is the equilibrium status. Because of the low friction coefficient of graphite additive sample, or the low energy input, the penetration of heat flux is small. Therefore, the thickness of deformed layer is small.

Second difference is that the maximum plastic deformation of the surface layer of graphite additive sample is bigger than that of the iron sample. this is also caused by lower friction coefficient. Under same normal pressure and sliding velocity, lower friction coefficient means lower friction force, which will result lower strain rate. Similar to the tensile test, lower strain rate will cause bigger elongation, plastic deformation of lower strain rate sample is bigger. When the material can stand higher plastic deformation, less debris will be generated, smaller wear rate will be achieved.

4.5 Effect of abrasive additive on plastic deformation

Abrasive particles in friction material can help to maintain wear resistance and high friction coefficient at elevated temperatures. The selection of abrasives should meet the requirements on service, cost and safety. In this project, the effect of abrasive

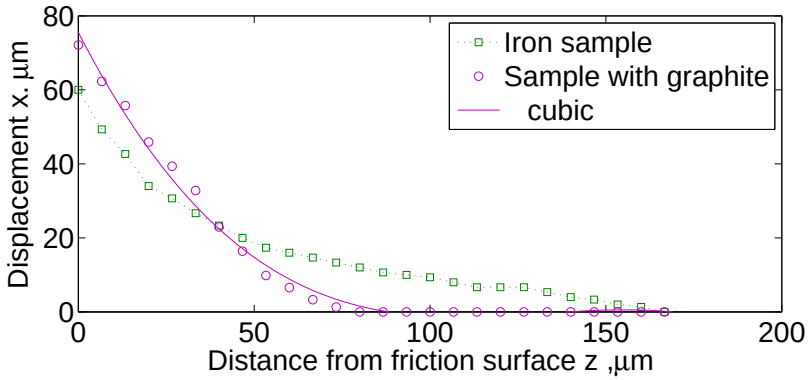

Figure 4.22: Effect of graphite on plastic deformation of matrix material

additive on the plastic deformation of matrix material is discussed. Silica (SiO_2) is chosen to be the abrasive additive. In order to minimize the geometric effect of an additive particle, quartz rod with 0.0635 inch diameter is used in the sample preparation.

Silica is brittle and it will crack during friction sliding. Fig 4.23 and 4.24 show the friction surface after test. Testing conditions are listed in Table 4.16. The difference between these two figures are that the quartz particle in s2 test is cracked. In Fig4.23, just a little matrix metal is deformed on the friction surface around the iron-silica boundary. Beside the deformed spot, no other deformation can be observed along the iron-silica boundary. In Fig 4.24, with the absence of a silica fragment, a different plastic deformation amount along the boundary can be observed at the void.

Due to thermal properties, silica particles will effect the temperature distribution of friction material during sliding. The thermal conductivity of silica is about 1.4

Table 4.16: Testing conditions of silica additive sample

Test	D (mm)	RPM (n/min)	v (m/s)	F (N)	μ	d (mm)	P (MPa)
s1	78.5	170	0.699	76.7	0.492	5	3.906
s2	78.5	130	0.534	88.8	0.461	5	4.523

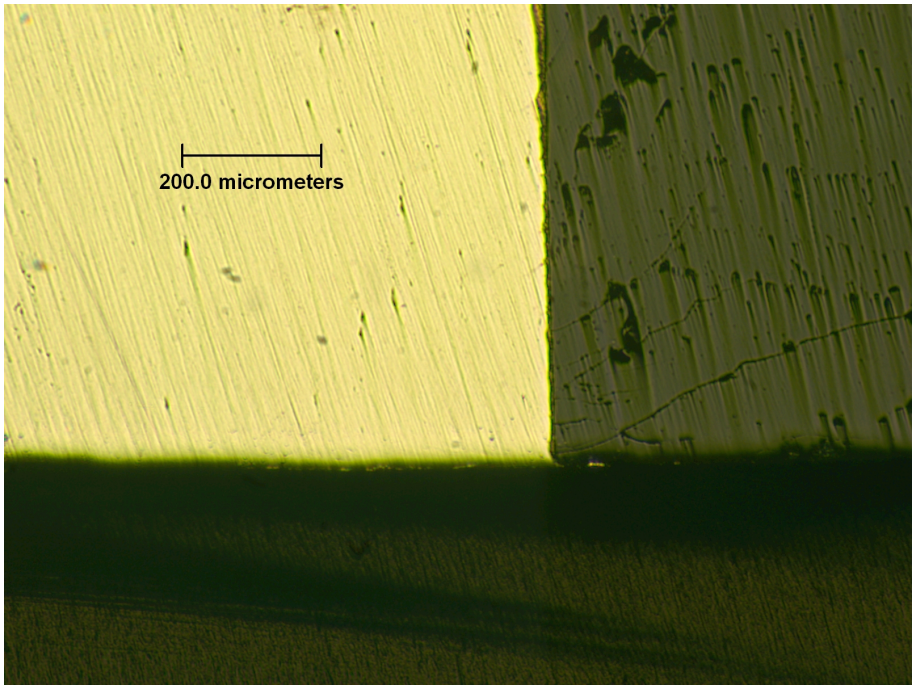

Figure 4.23: Friction surface after test s1 - without fragment of silica

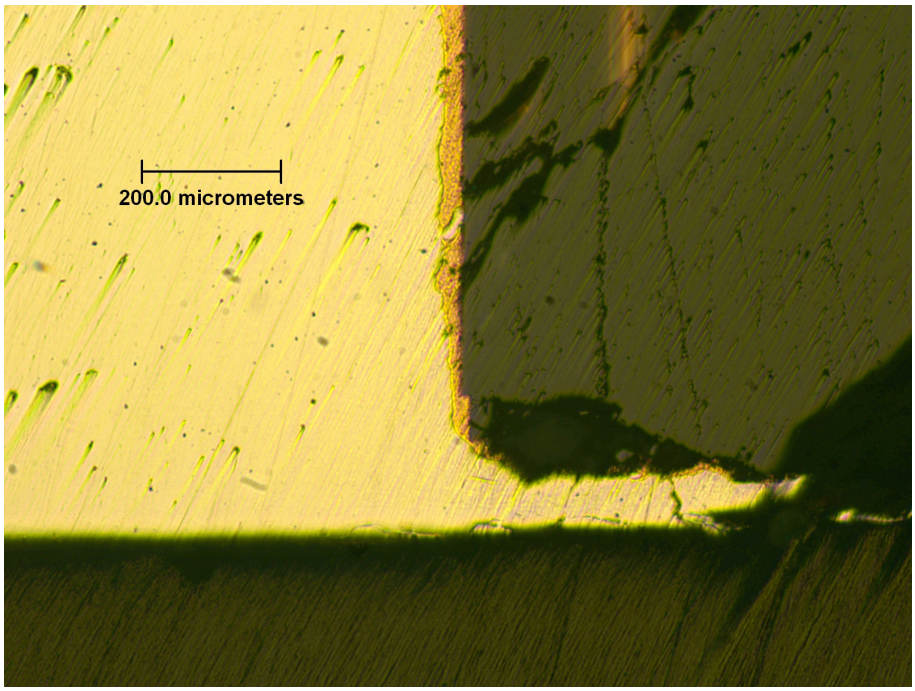

Figure 4.24: Friction surface after test s2 - with fragment of silica

$W/(m \cdot K)$, which is very small compare to that of iron (49.8 $W/(m \cdot K)$). It will result in heat accumulation on the friction surface. The effect of silica on temperature distribution is plotted in Fig 4.25. The simulation condition is the test condition of s1 test. The temperature of the matrix metal on the friction surface will be higher if there is a silica particle near the surface.

The lack of plasticity of silica is due to its covalent chemical bonds. the bonding between atoms involves the exchange of electron charge between pairs of electron. Thus, when silica is stressed to a sufficient load, it exhibit brittle fracture due to a separation of electron-pair bonds. In the friction test, the silica particle can be

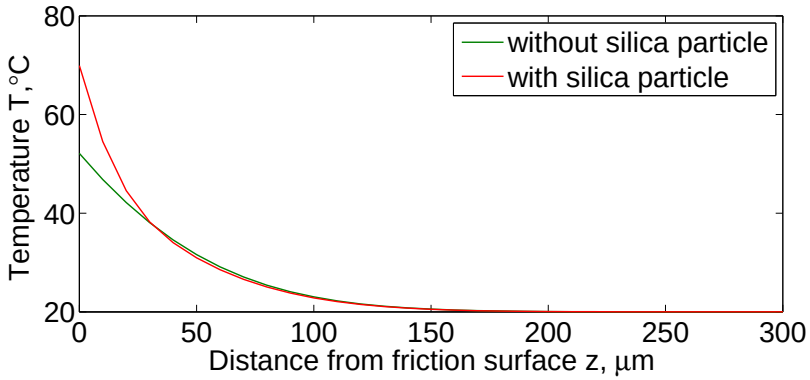

Figure 4.25: Effect of silica on temperature distribution

cracked but not deformed. The silica particle is extremely strong when it is supported by matrix metal. So when a friction force is applied, the matrix metal on the friction surface will be blocked by silica particle, so that no plastic deformation will occur.

Plastic deformation of matrix metal can only be observed on the friction surface when a silica particle is cracked and fragmented. Fragmentation of the silica particles is affected by several parameters such as the magnitude and direction of the load applied; the bonding condition between silica particle and matrix metal; and the surface flaws on the particles. Because each abrasive particle has a specific condition, the prediction of fragmentation of a single silica particle in a test specimen is difficult. In real friction materials, where thousand of abrasive particles are embedded, the fragmentation will be a statistical problem. This problem is under consideration for future study through.

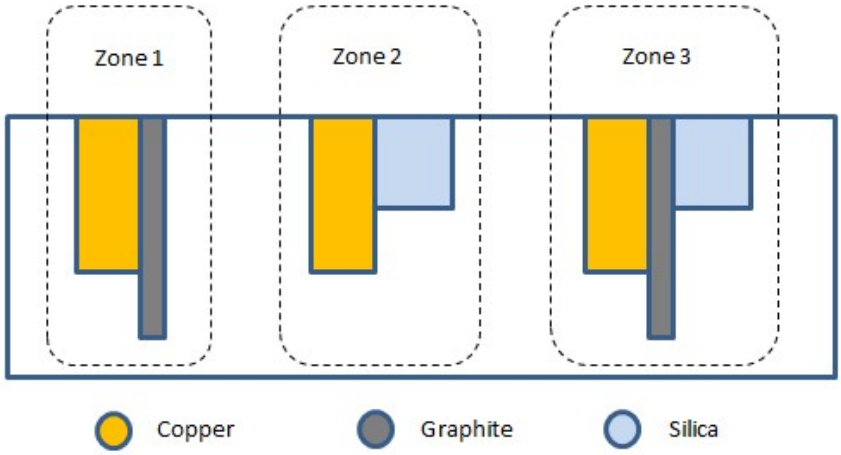

Figure 4.26: Schematic diagram of multi-additive model

4.6 Analysis of multi-additive model

After the study of a single additive effect, situations with multiple additives in matrix metal should be considered. Models with two or more additive particles should be studied next. A model of matrix material with more additive particles can be presented as in schematic drawing (Fig 4.26).Zone 1-3 present three different situations.

Zone 1 is the situation that have copper and graphite particles in matrix metal which is similar to the single copper particle model, but have a graphite particle. The graphite particle will effect the single copper particle model by modifying the friction coefficient and changing the surrounding geometry. During friction sliding, the deformation of matrix material and copper particle will squeeze the graphite out

and form a lubricant layer on the friction surface, which will decrease the friction coefficient. Then, the heat flux transfer into the friction material will decrease as well. The decreased heat flux, associated with the changed thermal properties which is caused by the introduction of graphite, will effect the temperature distribution of the surrounding area, effecting the plastic deformation. Because graphite is soft material, it cannot hold high pressure and cannot block the deformation of adjacent material. The graphite particle is like a void from the view of mechanical properties. Based on the analysis, model of zone 1 could be simplified to a single copper particle model with modified heat flux and thermal properties.

Compare the two simulations in Fig 4.27, close to the friction surface the multiple additives model has smaller amount of plastic deformation. That is because the copper, which has higher thermal conductivity, transfer more heat to the deeper layers. Therefore, in the graphite and copper additive model, the temperature of the surface layer is lower than that of graphite additive model.

The multiple additive model simulation is close to the test result, but error still exist. The deformed layer depth of simulation result is greater. From the analysis of uniform material model in Chapter 3, one can tell that this difference could be the affect by sliding velocity and thermal conductivity of material.

For a certain sliding distance, higher sliding velocity will cause higher energy input in a shorter time. Therefore the heat will accumulated at the friction surface, cause

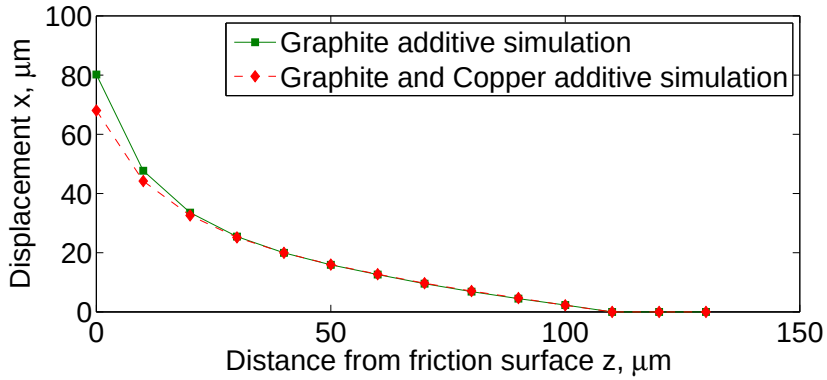

Figure 4.27: Simulation of graphite and copper additive model

a high deformation amount on the friction surface and shallow deformed layer depth. Thermal conductivity affects the plastic deformation in the opposite way. Higher thermal conductivity will transfer more heat into the material. So a small amount of deformation on the surface and deep deformed layers are expected.

Thermal conductivity is a material property which changes with temperature and composition of material. In the experiment, there are three factors that affect the heat transfer. First, the thermal conductivity data used in simulation is that under room temperature. During sliding, the thermal conductivity will be changed due to the elevated temperature. Second, the specimen was heating to a high temperature in order to obtain a good bond between additive particle and matrix material. During heating, the composition of matrix material will be changed. For example, the carbon will diffuse from graphite to iron under high temperature. Third, the distribution of real contact areas and friction layer formed on the friction surface will affect the heat

transfer as well.

Zone 2 in Fig 4.26 is presenting a copper particle and a silica particle in matrix material. From previous research of silica particle model, the silica particles will block the deformation of nearby material. So, assume that the silica particle is not cracked under friction load, an anticipation that no plastic deformation will be observed around the silica particle will be made. But, due to the different thermal properties, the introduction of silica particle will effect the temperature distribution of the nearby material. And the projection effect of silica particle will affect the load distribution of nearby material, therefore affect the heat flux. These two effects are not suppose to change the plastic deformation around the silica particle, but will more or less affect the adjacent area.

With Three different particles in matrix material, the model of zone 3 will be more complicated. In zone 3, the copper particle and it's neighbor matrix material will be deformed due to the graphite particle's attendance. And the plastic deformation will be affected by lower friction load which is cause by lubrication of graphite and projection of silica.

4.7 summary

This chapter is focused on the plastic deformation of composite models under friction load. Single particle additive models are discussed. Samples with different

additives were prepared and tested.

The simulation results of the copper additive model were compared with test results, and gave a good prediction. The graphite additive model gave a reasonable result which explained the effect of lubricant on plastic deformation. The test results of silica particle samples present the effect of abrasive particles on plastic deformation under friction load.

CHAPTER 5

CONCLUSIONS, CONTRIBUTIONS AND FUTURE WORK

In this chapter, the conclusions and main contributions resulting from these research activities are summarized. This is followed by some recommendations regarding possible research directions for future work.

5.1 Summary and Conclusions

This dissertation focused on the study of plastic deformation modeling of friction materials under high energy input. In Chapter 1, the problem background regarding this research topic was introduced. Through a literature search, the difficulties in friction mechanism research were reviewed. This includes overlapped processes during friction sliding; complexity of friction materials; and difficulty of synchronous observation. Based on this literature search, the main objectives of this work were delineated.

In chapter 2, the overview of processes during friction sliding, and the mechanism of plastic deformation during friction process were summarized. The processes such as plastic deformation of matrix material; oxidation of friction material; formation of friction layer; hot spot creation and mechanical mixing were reviewed. Their effects on each other were discussed also. Powder metallurgy friction materials were introduced,

as well as the effect of components and manufacturing of friction materials on friction performance.

Chapter 3 is mainly presenting the research of plastic deformation during friction sliding. A model of single material was established based on the study of material properties; the analysis of friction load and temperature distribution during friction. The model considered both the thermal softening caused by friction heat and the work hardening caused by plastic deformation. With the input of friction load and material properties of friction couple, the model could gave a prediction of plastic deformation of surface material during friction sliding. Specimen and experiments were designed to validate the model. Special specimen which is made od AISI 1045 steel and has a copper layer at the center of the cylinder shape was designed. The copper layer was used to indicate the deformation amount and distribution. The comparison of simulation results and test results demonstrated satisfactory accuracy of the model. Besides, The model of single material can also be used to study the effect of material properties and test conditions on plastic deformation via simulation of different situation.

Friction materials are composite materials. The components affect each other during friction sliding. Thus, simulation model of composite materials are discussed in chapter 4. The distribution and properties of different additive will effect the plastic deformation of friction material at the same time during friction sliding, which led to

the incomplete and incorrect understanding of their effects. In this chapter, specimens with single additive particles were prepared. The matrix material is AISI 1045 steel, and these additives include copper, graphite and silica. Copper additive specimen were used to study the effect of reinforcement filler particle on plastic deformation of matrix material; graphite additive specimen and silica additive specimen are for lubricants and abrasive particles forfriction enhancement.

Temperature distribution and plastic deformation of single additive model is established in chapter 4. The simulation results of single additive model can present the test results of copper additive specimens with satisfactory accuracy. Simulation model for graphite additive specimen is reasonable, and can be used to study the effect of lubricant. But with poor bonding between steel and graphite particle, the model cannot give accurate prediction.

5.2 Contributions

The main contribution resulting from this dissertation's work can be summarized as follow:

1. In order to build a model to study the plastic deformation during friction sliding, an algorithm based on Ramberg-Osgood relationship is generated. The models are build based on this algorithm, and validated by test results. The simulation model for single material could be used to study the effect of material

properties and friction load conditions on the plastic deformation, and gave a good prediction about plastic deformation based on the information input. In this model, thermal softening effect was considered. The material properties at elevated temperature were studied and a relationship between temperature and yield stress is built.

2. One additive particle models were build based on the single material model, and different additives were considered. The most common ones like graphite and silicon were used in experiments. This simple composite model was validated by experiment results and explained the effect of lubricant and abrasive particles.

In addition to the above mentioned main contributions, this dissertation also contributed to the following:

First, due to the expensive costs on the friction test machine, a simple pin on drum testing apparatus was built. The RPM of the drum is set by lathe setting and the sliding velocity of the pin specimen is decided by the RPM and the diameter of the drum. The friction load is adjusted by the springs on adjust bar, and measured by the FS6-120A load cell. Details are described in chapter 3 and shown in Fig 3.16.

Second, in order to observe the plastic deformation of specimen after friction test, some indicator should be used. To fulfill this requirement, two special specimen are designed. The specimen used for single material model study has a copper layer in the middle of specimen, and the one for additive model had a single additive particle in

the specimen. The design and manufacturing details of these specimen are described in chapter 3 and 4.

5.3 Possible Future Work

Based on the research results and progress obtained from this dissertation, several possible research directions in continuation of this work should be considered. Some of this future work may include the following:

1. The effect of abrasive particle on plastic deformation of matrix material as a statistical problem has not been investigated. During friction sliding, the abrasive particles will crack and the fragment of abrasive particle will effect the plastic deformation of surface material of friction couples. So the abrasive particle will not only affect the plastic deformation of adjacent matrix material, but also the material of other area.

2. The algorithm used in the simulation has several assumptions. In the temperature distribution calculation of a single additive model, for example, the temperature of any layer was assumed to be same at any moment during friction sliding. Improvements of assumptions will increase the accuracy of the simulations.

3. In this dissertation, single material model and single additive particle model were established. In order to simulate the plastic deformation of whole friction

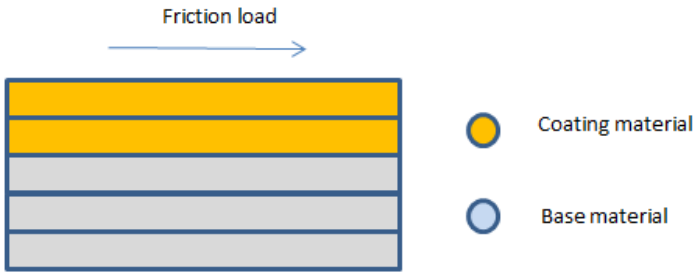

Figure 5.1: Schematic drawing of coating surface

material system, all of the additives should be considered during modeling. So the next step will be building the models for more additive particles.

4. In the single additive model, two different materials are vertically next to each other, which is similar to the situation of friction surface of composite friction materials. A model with two materials horizontally bonded could be used to simulate the plastic deformation of a coating surface. Fig 5.1 shows the schematic drawing of coating surface.

BIBLOGRAPHY

[1] I. U. W. Osterle, H. Kloss and A. I. Dmitriev, "Towards a better understanding of brake friction materials," *Wear*, vol. 263, no. 7-12, pp. 1189–1201, 2007.

[2] S. V. K. Pradeep L. Menezesa, Kishorea, "Role of surface texture of harder surface on subsurface deformation," *Wear*, vol. 266, no. 1-2, pp. 103–109, 2009.

[3] H. H. A. T. Alpas and J. Zhang, "Plastic deformation and damage accumulation below the worn surfaces," *Wear*, vol. 162-164(part A), pp. 188–195, 1993.

[4] V. L. Popov and S. G. Psakhie, "Physical nature and properties of dynamic surface layers in friction," *Tribology International*, vol. 39, no. 5, pp. 426–430, 2006.

[5] S. T. V. Panin, S. Kolubaev and V. Popov, "Subsurface layer formation during sliding friction," *Wear*, vol. 249, no. 10-11, pp. 860–867, 2001.

[6] V. R. S. Tarasov and A. Kolubaev, "Subsurface shear instability and nanostructuring of metals in sliding," *Wear*, vol. 268, no. 1-2, pp. 59–66, 2010.

[7] T. G. W. Osterle, M. Griepentrog and I. Urban, "Chemical and microstructural changes induced by friction and wear of brakes," *Wear*, vol. 251, no. 1-12, pp. 1469–1476, 2001.

[8] W. Osterle and I. Urban, "Friction layers and friction films on pmc brake pads," *Wear*, vol. 257, no. 1-2, pp. 215–226, 2004.

[9] ——, "Third body formation on brake pads and rotors," *Tribology International*, vol. 39, no. 5, pp. 401–408, 2006.

[10] W. Z. F. Peter and R. David, "On friction layer formation in polymer matrix composite materials for brake applications," *Wear*, vol. 252, no. 3-4, pp. 189–198, 2002.

[11] V. E. Rubtsov and A. V. Kolubaev, "Study of plastic shear deformation in surface layer at friction. simulation results. part i. model description," *Journal of Friction*

and wear, vol. 28, no. 1, pp. 65–78, 2007.

[12] ——, "Study of plastic shear deformation in surface layer at friction. simulation results. part ii. effect of friction parameters," *Journal of Friction and wear*, vol. 28, no. 2, pp. 173–181, 2007.

[13] W. O. A.I. Dmitriev, "Modeling of brake pad-disc interface with emphasis to dynamics and deformation of structures," *Tribology International*, vol. 43, no. 4, pp. 719–727, 2010.

[14] L. D. Vinci, *The notebooks of Leonardo da vinci.* compiled by Edward Maccurdy, George Braziller, 1954.

[15] P. Frederic, "what about friction?" *American Journal of Physics*, vol. 17, no. 6, pp. 181–187, 1949.

[16] B. Bharat and B. K. Gupta, *Handbook of tribology.* McGRAW-HILL, Inc., 1991.

[17] K. S. V. S. Dharmalingam, R. Subramanian, "Analysis of dry sliding friction and wear behavior of aluminum-alumina composites using taguchis techniques," *Journal of Composite Materials*, vol. 44, no. 18, pp. 2161–2177, 2010.

[18] E. Rabinowicz, *Friction and Wear of Materials.* John Wiley & sons, Inc., 1995.

[19] G. A. Tomlinson, "A molecular theory of friction," *Philosophical Magazine*, vol. 7, no. 46, pp. 905–939, 1929.

[20] F. P. Bowden and D. Tabor, "The area of contact between stationary and between moving surfaces," *Proc. Roy. Soc. A*, vol. 169, no. 938, pp. 391–413, 1938.

[21] J. W. M. F. P. Bowden and D. Tabor, "The plowing and adhesion of sliding metals," *Journal of Applied Physics*, vol. 14, pp. 80–91, 1943.

[22] J. M. J.T. Oden, "Models and computational methods for dynamic friction phenomena," *Computer Methods in Applied Mechanics and Engineering*, vol. 52, no. 1-3, pp. 527–634, 1985.

[23] D. A. Rigney, "Comments on the sliding wear of metals," *Tribology International*, vol. 30, no. 5, pp. 361–367, 1997.

[24] P. H. S. T. M. G. Jacko and S. K. Rhee, "Wear debris compaction and friction film formation of polymer composites," *Wear*, vol. 133, no. 1, pp. 23–38, 1989.

[25] K.-W. D. L. John, J. Young and R. Hull, "the generation of mechanically mixed layers (mmls) during sliding contac and the effects of lubricant thereon," *Wear*, vol. 246, no. 1-2, pp. 74–90, 2000.

[26] M. Godet, "the third-body approach: a mechanical view of wear," *Wear*, vol. 100, no. 1-3, pp. 437–452, 1984.

[27] D. E. A. Wirth and R. Whitaker, "A fundamental tribochemical study of third body layer formed during automotive friction braking," *Wear*, vol. 179, no. 1-2, pp. 75–81, 1994.

[28] X. X. P. Yao, H. Sheng and B. Huang, "Worn surface characteristics of cu-based powder metallurgy brake materials for aircraft," *Trans. Nonferrous Met. Soc. China*, vol. 17, pp. 99–103, 2007.

[29] P. D. P. Sansen and D. Weichert, "Fracture parameter for thermoplasticity in the case of dilatation symmetry," *Int. J. of fracture*, vol. 111, pp. 61–66, 2001.

[30] A. E. Anderson and R. A. Knapp, "Hot spotting in automotive friction systems," *Wear*, vol. 135, pp. 319–337, 1990.

[31] J. W. R. T. Kao and A. Douarre, "Brake disc hot spotting and thermal judder: an experimental and finite element study," *Int. J. Veh. Des.*, vol. 23, no. 3-4, pp. 276–296, 2000.

[32] D. Tabor, *Hardness of metals.* Oxford: Oxford Univ. Press, 1951.

[33] J. S. Courtney and E. Eisner, "The effect of a tangential force on the contact of metallic bodies," *Proc. Roy. Soc., A*, vol. 238, no. 1215, pp. 529–550, 1957.

[34] V. Prakash, "A pressure-shear plate impact experiment for investigating transient friction," *Experimental Mechanics*, vol. 35, no. 4, pp. 329–336, 1995.

[35] T. A. Stolarski, *Tribology in machine design.* Heinemann Newnes, 1990.

[36] P. Heilmann and D. A. Rigney, *Friction and wear.* J. K. Hirvonen, Ed., Trevi, Italy, NATO Workshop, 1981.

[37] P. K. Rohatgi, *Friction and wear of metal-matrix composites.* vol. 18, ASM Handbook, 1992.

[38] A. Nadkarni, *copper powder metallurgy alloys and composites.* vol. 7, ASM Handbook, 1992.

[39] N. A. Hooton, "Metal-ceramic composites in high-energy friction applications," *Technical Journal*, pp. 55–61, Spring 1969.

[40] G. Nicholson, *Facts About Friction.* Croydon, PA: P&W Price enterprises, Inc., 1995.

[41] M. Eriksson and S. Jacobson, "Tribological surfaces of organic brake pads," *Tribology International*, vol. 533, no. 12, pp. 817–827, 2000.

[42] P. Y. S. L. B. H. Xiang Xiong, Jie Chen, "Friction and wear behaviors and mechanisms of fe and sio2 in cu-based p/m friction materials," *Wear*, vol. 262, no. 9-10, pp. 1182–1186, 2007.

[43] R. T. Spurr, "Fillers in friction materials," *Wear*, vol. 22, no. 3, pp. 367–372, 1972.

[44] H. S. J. B. A. M. M. A. I. W. M. W. Ruzaidi, C. M.; Kamarudin, "Review of material used in brake pads," *International Review of Mechanical Engineering*, vol. 7, no. 3, p. 425, 2013.

[45] R. P. A. Nzihou, B. Adhikari, "Effect of metal chlorides on the sintering and densification of hydroxyapatite adsorbent," *Ind. Eng. Chem. Res.*, vol. 44, no. 6, pp. 1787–1794, 2005.

[46] X. Xiong, "Effects of sintering pressure and temperature on microstructure and tribological characteristic of cu-based aircraft brake material," *Trans. Nonferrous Met. Soc. China*, vol. 17, pp. 669–675, 2007.

[47] B. V. S. P. Bogdanovich, P.N., "Thermal processes in the contact of rubbing solids," *J. of friction and Wear*, vol. 13, no. 4, pp. 36–42, 1992.

[48] D. Buckley, *Surface Effects in Adhesion, Friction, Wear and Lubrication.* Amsterdam:Elsevier, 1981.

[49] D. P. Frank P.; DeWitt, *Fundamentals of heat and mass transfer*. John Wiley& Sons, 2002.

[50] O. Zmeskal, "Hot hardness testing," *Metal Progress*, vol. 51, no. 1, 1947.

[51] M. M. Yovanovich, "Micro and macro hardness measurements, correlations, and contact models," in *44th AIAA aerospacr Meeting and Exhibit*, 2006.

[52] W. R. Ramberg, W.; Osgood, "Description of stress-strain curves by three parameters," Technical Note No. 902, National Advisory Committee For Aeronautics, Tech. Rep., 1943.

[53] A. S. G.-. (2013), "Standard test method for pin abrasion testing." West Conshohocken, PA: ASTM International, 2013, DOI: 10.1520/G0132. http://www.astm.org.

[54] S. J. C. G. K. White, "Heat capacity of reference materials: Cu and w," *J. Phys. Chem. Ref. Data*, vol. 13, pp. 1252–1258, 1984.

[55] B. C. T.J. Miller, S.J. Zinkle, "Strength and fatigue of dispersion-strengthened copper," *Journal of Nuclear Materials*, vol. 179-181, pp. 263–266, 1991.

[56] F. A. I. Yasar, A. Canakci, "The effect of brush wpring pressure on the wear behaviour of copper-graphite brushes with electrical current," *Tribology International*, vol. 40, pp. 1381–1386, 2007.

APPENDIX I: Matlab code for Temperature distribution calculation

```
function T=temperatureppt(t,z)
global a b c d m = 0;
z = 0:b:a; t = 0:d:c;
sol = pdepe(m,@pdex1pde,@pdex1ic,@pdex1bc,z,t);
T = sol(:,:,1) -273.15;

function [c,f,s] = pdex1pde(z,t,T,DTDz)
global rho Sheat lambda
c=rho*Sheat/lambda;
f = DTDz;
s = 0;

function T0 = pdex1ic(z)
T0 = 293.15;

function [pl,ql,pr,qr] = pdex1bc(zl,Tl,zr,Tr,t)
global cof P Vcb lambda
w=0.5*cof*P*Vcb;
pl=w/lambda;
ql=1;
pr=Tr-293.15;
qr=0;
```

APPENDIX II: Matlab code for plastic deformation calculation

```
clear all
RCA=0.04;
global P cof Pnom Vcb rho Sheat lambda G0 theta0 a b c d
%a is the hight of asperities, b is the thickness of layers
%c is the length of contacting time, d is the length of time
    slice.
%e is the number of layers, f is the number of time slices
Pnom=5.271e6;P=Pnom/RCA; cof=0.2;Vcb=1.002;
%Test condition
rho=7872;Sheat=486; lambda=49.8;G0=80000;theta0=585;
%Material properties of AISI 1045
a=2e-2; b=1e-5; d=1e-3;c=2; e=round(a/b); f=round(c/d);
%setting of model
T=temperatureppt;
%Calculation of temperature distribution
G=(-63.694*T+81023)*1e6; theta=(-0.4658*T+592.48)*1e6;
%Temperature dependence of mechanical properties
gamma0el=sqrt((theta.^2-P^2)./(3*G.^2)); tau=P*cof; gammael=
    zeros(f+1,e+1);
gammapl=zeros(f+1,e+1); gammarate=zeros(round(f+1),round(e+1)
    ); gamma=tau./G;
srs=0.05; n=5; for j=1:e+1
        if gamma(1,j)<gamma0el(1,j) gammael(1,j)=gamma0el(1,j
            );
        else gammapl(1,j)=0.002*(tau/(gamma0el(1,j)*G(1,j)))^
            n;
             gammael(1,j)=gamma(1,j);
```

```
        end if gamma(2,j)<gamma0el(2,j)
            gammael(2,j)=gamma0el(2,j); else
        gammapl(2,j)=0.002*(tau/(gamma0el(2,j)*G(2,j)))^n;
            gammael(2,j)=gamma(2,j); end
        gammarate(2,j)=((gamma(2,j)+gammapl(2,j))-(gamma(1,j)
          +gammapl(1,j)))/d;
end ct=2; while ((sum(gammapl(ct,:))==0 ||
 gammapl(ct,1)<3*ones(1))&&ct<f+1)...
          &&min(theta(ct,:))>P ct=ct+1;
    for j=1:e if gamma(ct,j)<gamma0el(ct,j)
            gammael(ct,j)=gamma0el(ct,j); gammapl(ct,j)=
              gammapl(ct-1,j);
        else gammael(ct,j)=gamma(ct,j);
            gammapl(ct,j)=gammapl(ct-1,j)+tau/G(ct,j)+...
            0.002*(tau/(gamma0el(ct,j)*G(ct,j)))^n-gammael(
              ct,j);
        end gammarate(ct,j)=((gamma(ct,j)+gammapl(ct,j)))/(d*
          ct);
    end end
    el20el=zeros(f,e+1); for k=1:f
        el20el(k,:)=gammael(k+1,:)./gamma0el(1,:); end el20el
          =el20el';
    gammapl=gammapl'; T=T';
```